Review
doi.org/10.1002/elsa.202100090

Chemistry Europe
European Chemical Societies Publishing

Received: 19 May 2021
Revised: 17 June 2021
Accepted: 19 June 2021

Cathode strategies to improve the performance of zinc-ion batteries

Pingge He | **Shaowei Chen**

Department of Chemistry and Biochemistry, University of California, Santa Cruz, California, USA

Correspondence
Shaowei Chen, Department of Chemistry and Biochemistry, University of California, 1156 High Street, Santa Cruz, California 95064, USA.
Email: shaowei@ucsc.edu

Funding information
Beijing Natural Science Foundation, Grant/Award Number: 2204086; National Science Foundation, Grant/Award Numbers: CHE-1900235, CHE-2003685

Abstract

Zinc-ion battery (ZIB) has been attracting extensive attention due to its high theoretical capacity, high safety, and low cost. However, the exploration of suitable cathode materials to host Zn ions remains a challenge, owing to the strong electrostatic interactions and large steric hindrance effects between Zn ion and host materials. Great efforts have been devoted to the optimization of the structure and electrochemical property of the cathode materials. In this review article, we summarize recent cathode-based strategies to address the issues of performance degradation and structural collapse of electrode materials within the context of microstructure design and ion/charge transport mechanism, and include a perspective to highlight the challenges and promises in the exploitation of cathode materials for further enhancement of the performance of ZIBs.

KEYWORDS
cathode material, energy density, rate capacity, structural engineering, zinc ion battery

1 | INTRODUCTION

The development of rechargeable batteries plays an essential role in the area of energy conversion and storage. In the past few decades, lithium-ion batteries (LIBs) have dominated both academic and industrial research, due to their high energy density and long cycle life.[1–3] However, the practical application of LIBs is compromised by the safety issues, limited lithium resources, and environmental concerns.[4,5] Thus, research efforts have also been devoted to the development of alternative battery systems based on Na and K ions; nevertheless, safety issues remain a bottleneck.[6,7] Recently, novel multivalent-ion battery systems based on aqueous electrolytes rather than organic electrolytes have been regarded as promising candidates as the next-generation power supplies to meet the sustainable development of renewable energy in the modern era.[8] Among them, zinc-ion batteries (ZIBs) have gained intensive attention, since zinc-metal anode exhibits a high theoretical capacity (specific capacity 819 mAh/g), a low redox potential (−0.763 V vs. standard hydrogen electron [SHE]), and relatively high stability in aqueous electrolytes,[9,10] and has found preferable applications in high-performance aqueous batteries due to its environmental friendliness, low cost, and high safety.[11]

However, the fabrication of suitable cathode materials for ZIBs with a high reversible capacity, wide working voltage, and outstanding cycle stability remains a daunting challenge.[12] Divalent Zn^{2+} ions show strong electrostatic interactions with the host structures and large steric hindrance effects, leading to poor cyclic stability and sluggish intercalation kinetics. Thus, the design rules for the cathode materials of ZIBs are fundamentally different, as compared to that of monovalent ions-based

Review
doi.org/10.1002/elsa.202100090
Chemistry Europe
European Chemical Societies Publishing

batteries. Various types of materials have been used as cathodes for ZIBs,[13] such as manganese-based oxides, vanadium-based oxides, Prussian blue analogues (PBAs), and organic compounds; however, common issues related to cathode dissolution, electrochemical performance degradation, and structural collapse during cycling persist in these cathode materials.[10] Essentially, the performance of the cathode materials is closely related to their microstructures. Therefore, a profound understanding of the correlation between the material microstructure and energy storage mechanism is urgently needed so as to improve the cathode performance.

Recently, a series of reviews have been published on ZIBs, e.g., the introduction of cathode materials as well as their synthetic methods,[14] materials chemistry related to ZIBs,[15] energy storage mechanism,[16] layered oxide cathodes,[17] layered vanadium oxides,[18] manganese-based oxides,[19] microstructural engineering of cathode materials,[20] etc., while a comprehensive review on the optimization of cathode materials from the perspective of structural engineering, and the relationship with electrochemical property and ion/electron transport remains elusive and is urgently needed. Thus, in this review, we will first summarize recent progress where cathode-based strategies are exploited for improved ZIB performance, within the context of the cathode material structure and energy storage mechanisms. As schematically shown in Figure 1, the discussion will focus on the impacts of interlayer spacing, crystal structure, valence state, and morphology on the electrochemical properties of the cathode materials, and relevant strategies to improve the battery performance, such as intercalation of pillars, defect engineering, composite construction, nanostructure design, and heteroatom doping. Finally, a perspective is included to highlight future research directions for the development of cathode materials for high-performance ZIBs.

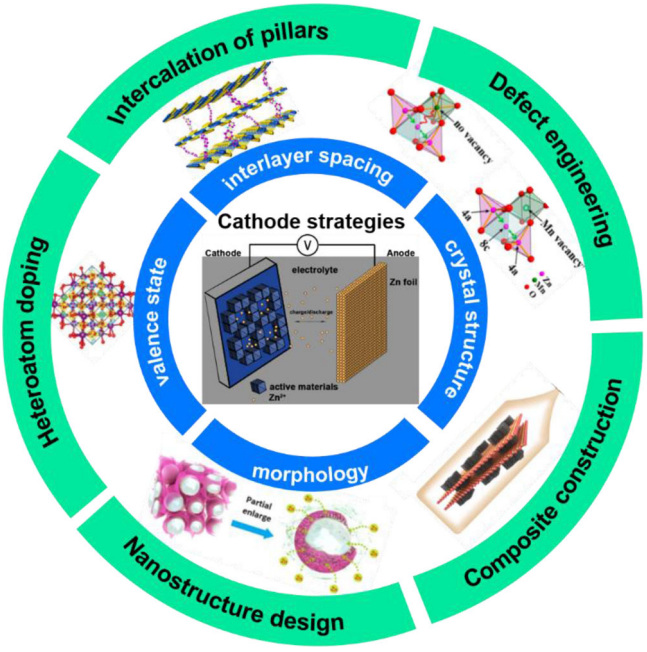

FIGURE 1 Cathode strategies to improve the performance of advanced ZIBs. Reproduced with permission from ref. [21], copyright 2018, Springer Nature; Reproduced with permission from ref. [22], copyright 2016, American Chemical Society; Reproduced with permission from ref. [23], copyright 2020, Wiley-VCH; Reproduced with permission from ref. [24], copyright 2019, American Chemical Society; Reproduced with permission from ref. [25]; copyright 2021, Elsevier

2 | TYPES OF CATHODE MATERIALS

Currently, there are mainly four types of cathode materials for ZIBs, Mn-based cathodes, V-based cathodes, PBAs, and organic materials. Among them, Mn- and V-based materials with tunnel or layered structures have been widely used in ZIBs.[26,27]

With a wide voltage window, high theoretical capacity, low cost, and environmental benignity, Mn-based materials, particularly manganese oxides, have attracted extensive attention as ZIB cathodes.[19] The Mn element shows rich valance states with various crystalline structures, such as MnO_2, Mn_2O_3, Mn_3O_4, and MnO. Among them, MnO_2 exhibits outstanding structural flexibility and can form various crystallographic polymorphs, such as α-, β-, γ-, δ-, λ-, R-, and ε-type,[10,28] by connecting the fundamental MnO_6 octahedral units that consist of one Mn^{4+} surrounded by six oxygen neighbors via the edges and/or corners. Typically, α-MnO_2 possesses a large tunnel structure of [2×2] along the c-axis with four edge-sharing MnO_6 octahedral units, β-MnO_2 shows [1×1] tunnels along the c-axis, γ-MnO_2 shows [1×1] and [1×2] hybrid tunnels along the b-axis (Figure 2), and δ-MnO_2 displays a layered structure with a large interlayer spacing.[10] Since the electrochemical performance highly depends on the crystal structure of the materials, the different polymorphs of Mn-based oxides exhibit varied electrochemical properties, and the ones with larger tunnels or interlayer spaces usually show a faster ion-diffusion capacity. Yet, the rate capability remains low and cycle life short for Mn-based oxide cathode materials, due to their low electronic conductivity and dissolution of Mn in electrolyte. Efforts to address these issues will be discussed in section 4.

Besides manganese, vanadium also displays rich valence states varying from +2 to +5, and when used as battery electrodes, exhibits a high charge/discharge capacity through the multielectron transfer processes. Recently, vanadium-based compounds with tunnel-type or layered structures have been used as promising cathode materials

Review
doi.org/10.1002/elsa.202100090
Chemistry Europe
European Chemical Societies Publishing

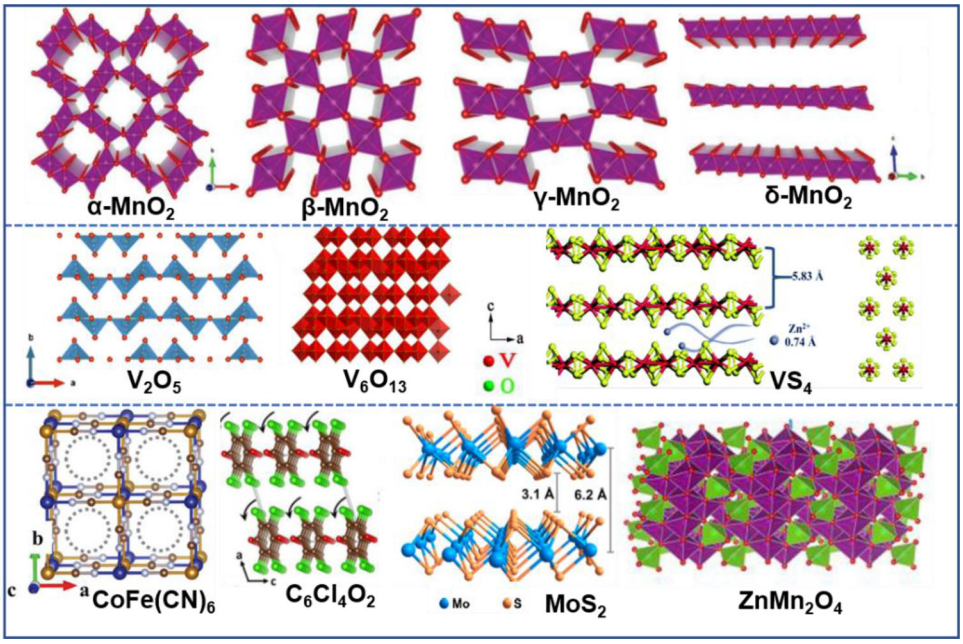

FIGURE 2 Crystal structures of different cathode materials, MnO_2 (reproduced with permission from ref. [28], copyright 2018, Wiley-VCH), V_2O_5 (reproduced with permission from ref. [29], copyright 2019, Elsevier), V_6O_{13} (reproduced with permission from ref. [30], copyright 2019, Wiley-VCH), VS_4 (reproduced with permission from ref. [33], copyright 2020, Royal Society of Chemistry), $CoFe(CN)_6$ (reproduced with permission from ref. [35], copyright 2019, Wiley-VCH), $C_6C_{l4}O_2$ (reproduced with permission from ref. [39], copyright 2018, American Chemical Society), MoS_2 (reproduced with permission from ref. [41], copyright 2019, American Chemical Society), and $ZnMn_2O_4$ (reproduced with permission from ref. [44], copyright 2019, Elsevier)

for rechargeable ZIBs. In particular, vanadium oxides, such as V_2O_5, VO_2, and V_6O_{13}, with a tunnel framework (Figure 2), have been widely used for ZIB applications.[29,30] In addition, mixed valence states in V-based oxides have been demonstrated to increase the redox reaction sites and thus enhance the capacity of the cathodes.[31] For example, V_6O_{13} with alternating single and double vanadium oxide layers consists of a mixed valence state of V^{5+}/V^{4+}, and offers a high number of active sites for ion storage. As a result, V_6O_{13} exhibits a high capacity and excellent cyclic stability.[30,31] Mixed vanadium valences have also been found to improve the electrochemical performance of V_2O_5. In comparison to pristine V_2O_5, the incorporation of V^{4+} into V_2O_5 leads to a higher electrochemical activity, lower polarization, faster ion diffusion, and higher electrical conductivity, which provides an effective way to design high-performance V-based oxide cathodes for ZIBs.[32] Moreover, V-based sulfides, such as VS_4, have also been employed as ZIB cathodes, due to the one-dimensional atomic chain structure (Figure 2).[33] Nevertheless, similar to Mn-based oxides, vanadium oxide cathodes usually experience dissolution and structural degradation during the charge/discharge process, leading to a poor cyclic performance.

PBAs ($MFe(CN)_6$, with M = Fe, Co, Ni, etc.) typically display a face-centered cubic (fcc) structure with a three-dimensional open framework and large ion-intercalation sites for rapid ions transportation (Figure 2),[34] and hence a great potential in aqueous ZIB applications.[35] PBAs like $CoFe(CN)_6$[36] are known to exhibit a high rate capability, but they suffer a low capacity and short cycle lifespan, which severely limits their wide applications in ZIBs. The low capacity of PBAs is attributed to the inactive sites in their structure,[36] and the poor cyclic stability originates from phase transformation during cycling.[37] Feasible strategies to mitigate these issues will be discussed in section 4.

Organic compounds have also been investigated as rechargeable ZIB cathodes, due to their light weight, structural flexibility, sustainability, low cost, multiple electron reactions, and biodegradable characters.[38,39] More importantly, organic materials with relatively weak intermolecular interactions can offer a sufficient space to accommodate zinc ions during cycling, leading to outstanding cyclic stability. However, organic compound cathodes usually suffer a low capacity and unstable voltage plateaus. For instance, Chen *et al.*[40] prepared a quinone (C4Q)-cathode for ZIBs which showed a high energy density. Unfortunately, to prevent the crossover of the soluble discharge product of the C4Q-cathode in this system, an expensive fluorine-containing membrane (Nafion film) must be used as the separator. Furthermore, the Nafion

separator must be tightly sealed to prevent the mixing of anolyte and catholyte, which is very difficult to be applied in flexible devices, especially when operated under repeated bending conditions. Further studies are needed to develop effective methods to optimize the structure and performance of organic cathode materials.

Other cathode materials, such as transition metal dichalcogenides (TMDs),[41] cobalt-based oxides,[42] molybdenum oxides,[43] and binary metal oxides,[44] have also been examined for ZIBs (Figure 2). Despite substantial progress, issues remain with these cathode materials, in particular, low capacity, low rate capability, and short cycle life. Thus, strategies to optimize the structure and improve the performance of cathode materials are urgently required for the further development of ZIBs.

3 | REACTION MECHANISMS OF ZIB CATHODES

Understanding the energy storage mechanism is critical in the rational design of cathode materials for an optimized electrochemical performance. In ZIBs, several reaction mechanisms have been proposed for energy storage of the cathode materials. Herein, the discussion will focus on three main ones, (1) Zn^{2+} intercalation/deintercalation mechanism, (2) conversion reaction mechanism, and (3) H^+/H_2O and Zn^{2+} co-insertion/extraction mechanism.

3.1 | Zn^{2+} intercalation/de-intercalation mechanism

Similar to LIBs, the energy storage in most cathodes of ZIBs depends on the intercalation/de-intercalation of Zn ions into/from cathode materials. Due to the small ionic radius (0.75 Å) that is comparable to that of Li^+, Zn^{2+} can effectively diffuse into/extract from a range of layered or tunnel-type host structures.[45,46] For example, in γ-MnO_2 (1×1 and 1×2 tunnels) cathode, during the insertion of Zn^{2+}, spinel-type $ZnMn_2O_4$ is initially produced, followed by tunnel-type γ-Zn_xMnO_2, and finally layered Zn_xMnO_2.[47] Besides MnO_2, Zn^{2+} intercalation/de-intercalation can also occur in layered or tunnel-type vanadium-based oxides, owing to their large ion-transfer channels, multiple oxidation states of vanadium, and high capacities (generally > 300 mAh/g).[48,49] Other materials, such as MoS_2,[50] MoO_3,[43] VS_2,[51] PABs with open frameworks, as well as NASICON-type phosphates,[52] have also been demonstrated as electroactive hosts for Zn^{2+} intercalation/de-intercalation.

For cathode materials with energy storage through the (de-)intercalation of Zn^{2+}, enlarging the interlayer spacing is a critical route to improve the electrochemical performance. Effective methods, such as intercalation of pillars, have been demonstrated to significantly increase the interlayer spacing of cathode materials and thus enhance their capacity and cyclic stability, which will be discussed in section 4.

3.2 | Conversion reaction mechanism

Different from materials that serve as hosts for Zn ion insertion/extraction, some cathode materials store energy based on conversion reactions. In this mechanism, phase transformation of the cathode materials usually occurs during charge/discharge. For example, α-MnO_2 cathode in a MnO_2/Zn battery has been demonstrated to transform to MnOOH during cycling, and such a phase transformation takes place in the presence of water.[53] The conversion reactions in the cathode can be described as follows,

$$H_2O \leftrightarrow H^+ + OH^- \quad (1)$$

$$MnO_2 + H^+ + e^- \leftrightarrow MnOOH \quad (2)$$

$$1/2Zn^{2+} + OH^- + 1/6ZnSO_4 + x/6H_2O \leftrightarrow 1/6ZnSO_4\left[Zn(OH)_2\right]_3 \cdot xH_2O + e^- \quad (3)$$

Such a conversion reaction mechanism has also been reported in other materials. For example, Chen *et al.*[42] prepared a Co_3O_4/Zn battery based on Co(III) rich-Co_3O_4 nanorods as cathode. During charge/discharge, the Co_3O_4 nanorods were transformed into CoO in aqueous electrolytes, and the Co(III) rich state in the cathode materials led to a highly effective reaction. Besides the structure of cathode materials, the operation voltage and electrolyte media (including ion concentration, pH, additive, and so on) also show significant influences on the conversion reaction process. Cathode materials based on the conversion reaction mechanism can be engineered to exhibit a large specific surface area, mixed valence-states, and controllable porous structure, so as to increase the accessibility by electrolytes, improve the reaction kinetics, and consequently enhance the discharge capacity and rate capability of the cathodes.

Review
doi.org/10.1002/elsa.202100090
Chemistry Europe
European Chemical Societies Publishing

3.3 | H^+/H_2O and Zn^{2+} co-insertion mechanism

Besides Zn^{2+}, protons (H^+) in an aqueous ZIB have been recognized as the main charge carrier, due to their small ionic radius and low atomic mass, and insertion/extraction of both H^+ and Zn^+ takes place concurrently during charge/discharge.[54,55] For instance, a unique H^+ and Zn^{2+} co-insertion mechanism has been proposed to account for the performance of a Zn/MnO_2 battery using a $ZnSO_4$-based aqueous electrolyte,[56] as $ZnMn_2O_4$ and MnOOH phases are both observed after discharge, due to the insertion of $Zn^{2+}$and H^+, respectively. As compared to Zn^{2+}, the smaller size of H^+ enables faster insertion kinetics, resulting in a big difference in the galvanostatic intermittent titration technique (GITT) profiles, where the H^+ intercalation process shows a much lower overvoltage at the first discharge platform than that of Zn^{2+} at the second platform.[56]

Furthermore, H_2O has also been demonstrated to play an essential role in the Zn^{2+} storage process. A unique Zn^{2+}/H_2O co-insertion storage mechanism has been revealed in a $Zn_{0.25}V_2O_5{\cdot}nH_2O/Zn$ battery.[57] When the cathode materials were immersed into the aqueous electrolyte, H_2O molecules would intercalate into pristine $Zn_{0.25}V_2O_5{\cdot}nH_2O$, leading to an increment of the interlayer distance. Then, in the discharge process, the H_2O molecules were de-intercalated from the cathode accompanied by Zn^{2+} intercalation, whereas during charging, intercalation of H_2O molecules occurred along with Zn^{2+} de-intercalation, leading to highly reversible and stable electrochemical operation.

Based on the co-insertion mechanism of energy storage, cathodes with structural H_2O and selection of suitable aqueous electrolytes are expected to enhance the electrochemical performance of ZIBs.

Other reaction mechanisms have also been proposed for ZIBs. For example, an "ion-coordination" mechanism was proposed by Chen *et al.*,[40] where C4Q was used as the cathode material and the carbonyl groups in C4Q acted as the active sites for Zn ion storage, as Zn^{2+} ions were coordinated to the electronegative oxygen atoms. In another study,[58] an anion intercalation/de-intercalation mechanism was revealed in a Zn/graphite battery system consisting of a zinc metal anode, graphite cathode, and 1 M zinc dibis (trifluoromethylsulfonyl)imide ($Zn(TFSI)_2$)/acetonitrile electrolyte. Energy storage in such a Zn/graphite battery was based on the (de)intercalation of $TFSI^-$ anion into the graphite (graphite$[TFSI^-]_x$) and the electrochemical plating/stripping of Zn^{2+} on the anode.

4 | STRATEGIES TO IMPROVE THE ELECTROCHEMICAL PERFORMANCE OF CATHODES

In ZIB applications, many cathode materials suffer electrochemical performance degradation during charge/discharge, due to dissolution, structural collapse, poor electrical conductivity, and sluggish transport kinetics.[59–61] To mitigate these issues and enhance the ZIB performance, a number of strategies have been examined to engineer the structure of the cathode materials.

4.1 | Intercalation of pillars

Based on the Zn^{2+} insertion/extraction mechanism, cathode materials are required to exhibit a large interlayer spacing to accommodate Zn ions. However, traditional cathodes usually exhibit only a limited interlayer spacing and unstable structure during Zn ion de/intercalation,[10,14] compromising their application as high-performance cathodes for ZIBs. Great efforts have been devoted to these issues, among which the most effective way is to intercalate metal ions,[62,63] polymers,[64,65] or molecular water (H_2O)[66,67] as pillars into the cathode materials to enlarge the interlayer spacing and enhance the structural stability during the charge/discharge process.

4.1.1 | Metal-ion intercalation

Metal-ion intercalation can be classified based on the kind of intercalated metal ions, i.e., transition metal ions, alkali metal ions, alkali-earth metal ions (Mg^{2+}, Ca^{2+}, etc.), and even aluminum ions (Al^{3+}). Wang *et al.*[63] reported that pre-intercalation of Zn^{2+} transformed layered δ-MnO_2 nanosheets into highly stable, tunnel-structured Zn_xMnO_2 nanowires (Figure 3A). This enabled fast kinetics and significantly improved the cycling performance of ZIBs with a high capacity-retention rate of 83.1% after 5000 cycles at 15 mA/cm^2 (Figure 3B).[63] Zn ions can also act as pillars for vanadate cathodes to enhance the cycle life and low-temperature behaviors.[68] After the first discharge process, the NH_4 ions in the $(NH_4)_2V_6O_{16}{\cdot}1.5H_2O$ (NVO) cathode were transferred into the aqueous electrolyte leaving enough vacancies behind for Zn ion intercalation. The trapped $Zn(H_2O)_6^{2+}$ ions in the interlayer not only helped stabilize the vanadium oxide layer but also provided enough interlayer spacing for fast ion kinetics during the subsequent insertion/extraction. As a result, the NVO cathode displayed a high specific capacity of 385 mAh/g,

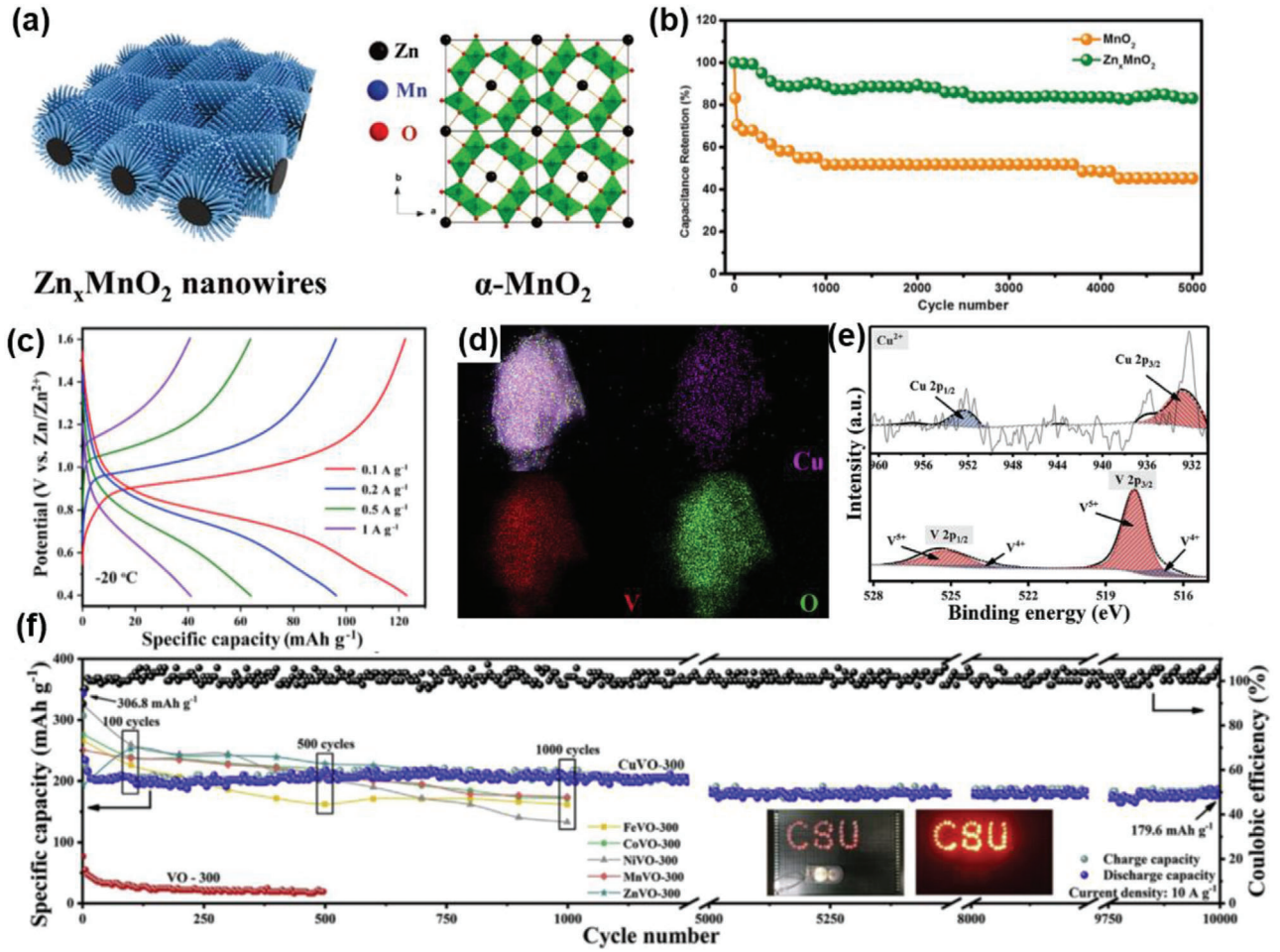

FIGURE 3 (A) Schematic diagram of the formation of Zn_xMnO_2 nanowires and their crystal structure. (B) Cycling performance of MnO_2 and Zn_xMnO_2 based ZIBs at 15 mA/cm^2 (reproduced with permission from ref. [63]; copyright 2020, Wiley-VCH). (C) Charge/discharge curves of a Zn/NVO battery in the 2nd cycle at varied current densities at a low temperature of −20°C (reproduced with permission from ref. [68]; copyright 2019, Elsevier). (D) TEM-EDX elemental mapping images and (E) XPS spectra of CuVO-300. (F) Long-term cycling performances of TVO-300 and VO-300 at 10 A/g with insets showing a lamp panel illuminated by four Zn/CuVO-300 coin cells (reproduced with permission from ref. [69]; copyright 2019, Elsevier)

and a good electrochemical performance even at low temperatures (Figure 3C).[68]

Besides Zn ions, other transition metal ions have also been used as effective pillars for cathode structure enhancement. Zhou *et al.*[69] demonstrated that chemical pre-intercalation of transition-metal ions (e.g., Fe^{2+}, Co^{2+}, Ni^{2+}, Mn^{2+}, Zn^{2+}, and Cu^{2+}) into the interlayer of V_2O_5 (TVO) could effectively improve the electrochemical performance of aqueous ZIBs, in terms of high capacity, rate capability, long-term cycling stability, as well as excellent broad temperature adaptability. The successful introduction of metal ions (particularly Cu ions, Figure 3D and E) into the V_2O_5 (VO) interlayers can not only drastically enhance the specific capacity, but also improve the structural stability during cycling, thus leading to a long cycle life and an ultrahigh capacity retention of 88% over 10,000 cycles (Figure 3F).

Meanwhile, alkali metal ions, such as Li, Na, and K, have also been demonstrated to improve the electrochemical performance of cathodes by tuning the electronic structure and stabilizing the material's layered structure. In a recent study,[70] Geng *et al.* fabricated K^+ pre-intercalated layered V_2O_5 ($K_{0.5}V_2O_5$) electrodes with metallic features and observed an excellent zinc storage performance. The optimized $K_{0.5}V_2O_5$ exhibited a Pmm2 symmetry structure with the K atom occupying the hollow site between two V_2O_5 layers (Figure 4A). Compared with pristine V_2O_5, $K_{0.5}V_2O_5$ expanded along the a and c directions, but shrank along the b direction, with a final volume of V_2O_5 slightly increased from 177 Å^3 to 187 Å^3 after the insertion of K ions. By analyzing the density of states (DOS), both the valence band edge and conduction band edge of $K_{0.5}V_2O_5$ showed a significant blue shift, resulting in the polarized and metallic band structure, as compared to that of V_2O_5

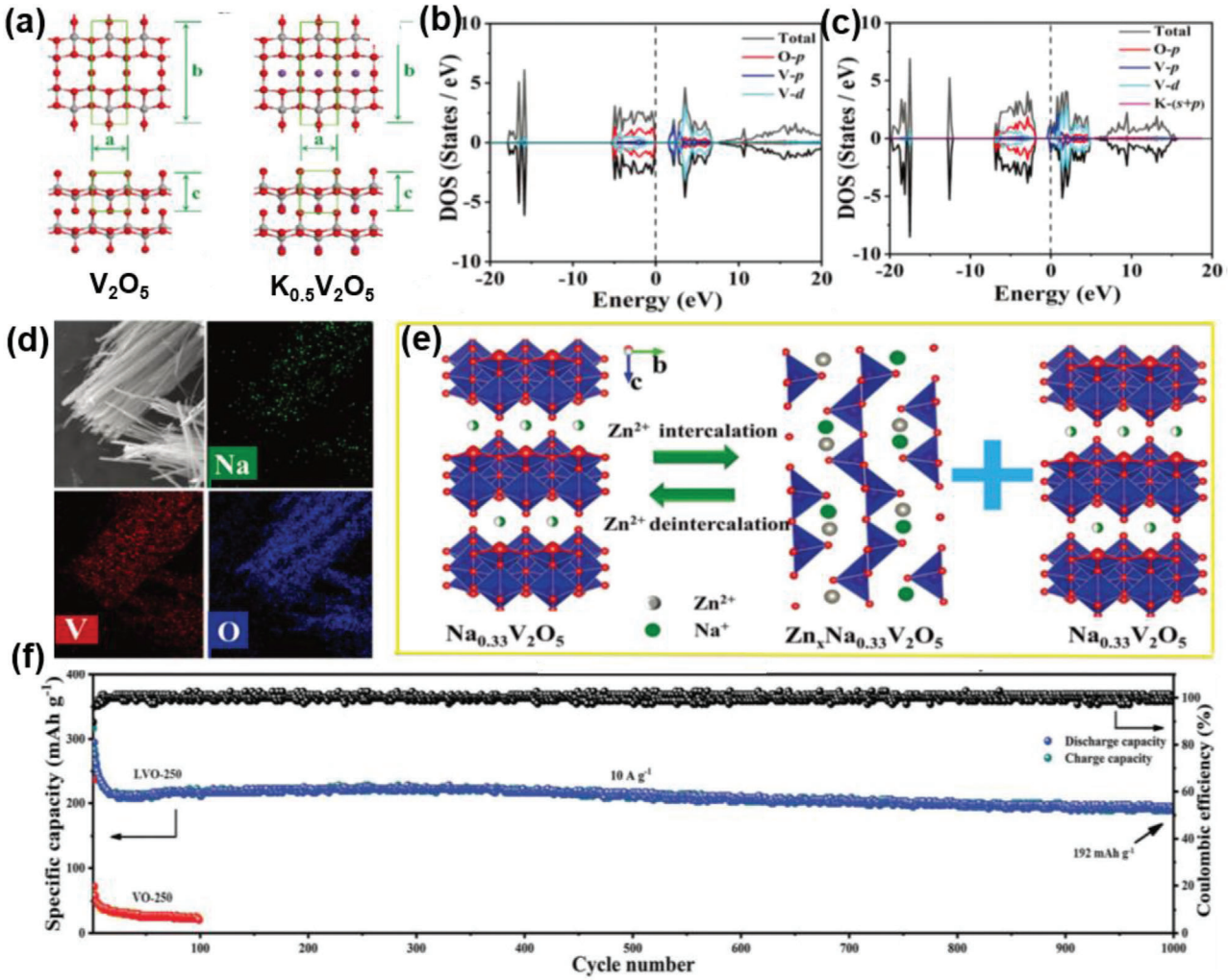

FIGURE 4 (A) Top and side views of V_2O_5 and $K_{0.5}V_2O_5$. The green frames indicate the unit cell. The red, grey, and purple spheres denote O, V, and K atoms, respectively. (B) DOS of V_2O_5. (C) DOS of $K_{0.5}V_2O_5$ (reproduced with permission from ref. [70]; copyright 2021, Royal Society of Chemistry). (D) SEM-EDX elemental maps of NVO nanowires. (E) Schematic illustration of the zinc-storage mechanism in the NVO electrode (reproduced with permission from ref. [71]; copyright 2018, Wiley-VCH). (F) Long cycling performances at 10 A/g of LVO-250 and VO-250 (reproduced with permission from ref. [72]; copyright 2018, Royal Society of Chemistry)

(Figure 4B and C). That is, the band structure of V_2O_5 was readily manipulated by K ion intercalation.[70] K^+ ions have also been employed as pillars for MnO_2, and the pre-intercalated K ions in the layered-type matrix have been demonstrated to stabilize the layered structures and expand Zn^{2+} migration channels, facilitating the diffusion of Zn^{2+} in the MnO_2 cathodes.[62]

In another study,[71] Mai's group prepared a $Na_{0.33}V_2O_5$ cathode for ZIBs and observed improved electrical conductivity, which was attributed to the intercalation of Na^+ into V_2O_5. From Figure 4D, one can see that the Na, V, and O elements were uniformly distributed, and no other element was detected. During charge/discharge (Figure 4E), Zn ions reversibly de/intercalated into the cathode structure, where the interlayer spacing was enlarged by the Na^+ pillars. Zhou *et al.* [72] proposed an effective strategy based on chemical intercalation of Li^+ into the interlayer of $V_2O_5{\cdot}nH_2O$ (VO), i.e., $Li_xV_2O_5{\cdot}nH_2O$ (LVO), to enlarge the layer spacing and enhance Zn^{2+} diffusion. As a cathode in aqueous ZIBs with a 2 M $ZnSO_4$ electrolyte, the LVO thermally annealed at the temperature of 250 °C (LVO-250) demonstrated a high rate capacity and excellent cycling performance, with a high capacity retention of 192 mAh/g after 1,000 cycles at 10 A/g (Figure 4F).

Moreover, alkali-earth metal ions have also been employed as pillars for cathodes with improved electrochemical performance. For instance, Alshareef *et al.*[73] prepared a layered Mg^{2+}-intercalated V_2O_5 as the cathode material for aqueous ZIBs. The large radius of hydrated Mg^{2+} led to an increased interlayer spacing of 13.4 Å, enabling efficient Zn^{2+} (de)insertion. As a result, the

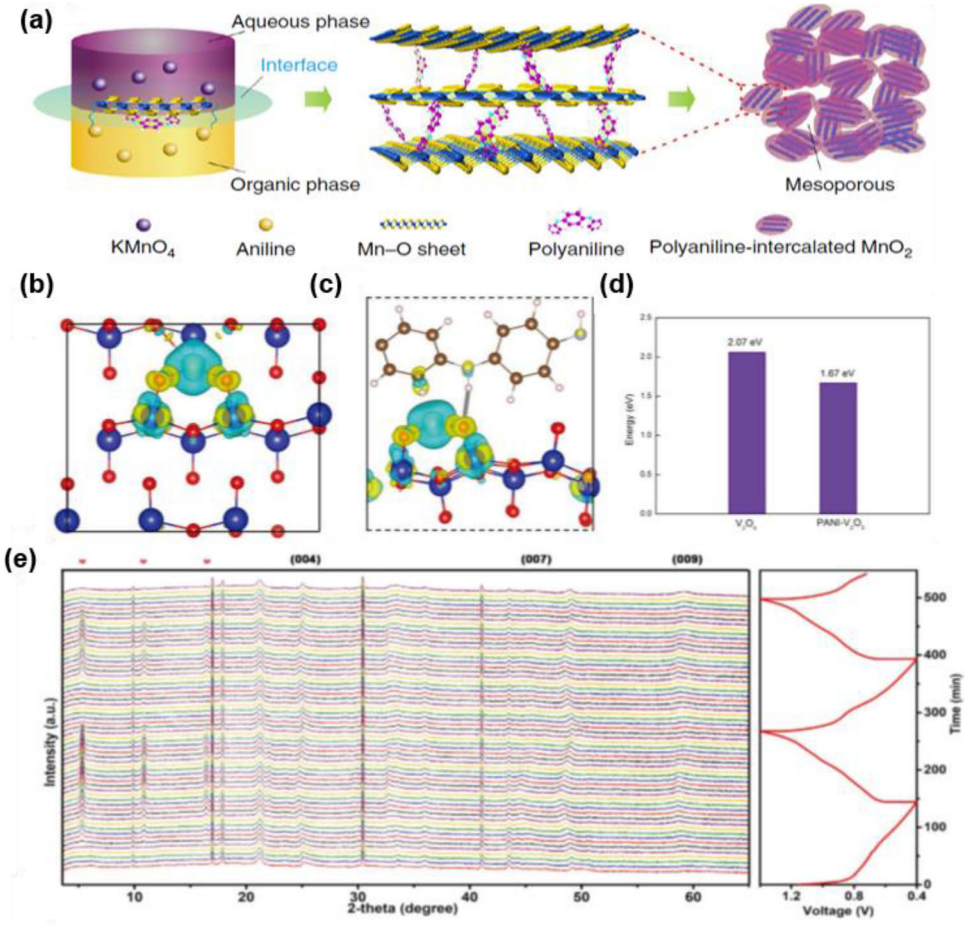

FIGURE 5 (A) Schematic illustration of the expanded intercalated structure of PANI-intercalated MnO_2 nanolayers (reproduced with permission from ref. [21]; copyright 2018, Springer Nature). Differential charge density with Zn-ion intercalation in (B) pristine V_2O_5 and (C) PANI-V_2O_5. The yellow and cyan regions represent charge accumulation and depletion, respectively. Blue, red, brown, light blue, gray, and white balls represent V, O, C, N, Zn, and H atoms, respectively. (D) Calculated binding energy of Zn ions inserted in V_2O_5 and PANI-V_2O_5 (reproduced with permission from ref. [78]; copyright 2020, Wiley-VCH). (E) In situ XRD tests of PANI100–V_2O_5 and the corresponding time–voltage curves (reproduced with permission from ref. [79]; copyright 2020, Wiley-VCH)

obtained porous $Mg_{0.34}V_2O_5{\cdot}0.84\,H_2O$ cathodes worked in a wide potential window of 0.1 to 1.8 V versus Zn^{2+}/Zn, and can deliver high capacities of 353 and 264 mAh/g at current densities of 100 and 1000 mA/g, respectively, along with long-term durability. Additionally, Zhang *et al.*[74] demonstrated that insertion of Ca^{2+} into hydrated vanadium oxide cathode expanded the layer spacing, greatly reduced the electrostatic interactions, and increased the reversibility of the vanadium oxide. Besides these alkali-earth metal ions, Al^{3+}[75] and even non-metallic NH^{4+}[76] ions have also been reported as effective pillars to optimize the structure of cathode materials.

Notably, these universal strategies based on pre-intercalated metal ions in the host materials have indeed been confirmed to enlarge Zn^{2+} diffusion channels, improve electrical conductivity, and stabilize the structure during cyclic charge/discharge, leading to fast Zn^{2+} diffusion, and long cycle life,[69] and can be applied to various types of cathode materials (e.g., MnO_2, V_2O_5, etc.) and advanced battery systems.

4.1.2 | Polymer intercalation

Besides metal ions, polymers have also been used as promising pillars to engineer the cathode structure.[77] For instance, Wang *et al.*[21] designed a polyaniline (PANI)-intercalated layered manganese dioxide as ZIB cathode and observed significantly improved cyclic stability. The sample was prepared via a one-step procedure where oxidative polymerization of aniline and reduction of MnO_4^- occurred simultaneously at the organic/inorganic interface, leading to the layer-by-layer assembly of MnO_2 and PANI (Figure 5A). Such a PANI-reinforced layered structure with nanosized MnO_2 particles (~10 nm) efficiently eliminated the hydrated H^+/Zn^{2+}

insertion-induced phase transformation and subsequent structural collapse, resulting in a long cycle life.[21]

Zhang *et al.*[65] designed a PANI-intercalated hydrated V_2O_5 composite (PANI/V_2O_5), in which PANI not only expanded the interlayer spacing (as large as 14 Å) of V_2O_5 for fast and reversible Zn^{2+} ion (de)intercalation, but also improved the specific capacity of the cathode materials. The as-assembled Zn//PANI/V_2O_5 battery exhibited a high specific capacity up to 353.6 mAh/g at 0.1 A/g, and a stable cycling performance. In another study,[78] Li's group developed an in-situ PANI intercalation strategy to facilitate the Zn^{2+} (de)intercalation kinetics in V_2O_5. They found that not only the interlayer spacing was significantly enlarged, but more importantly, the electrostatic interactions between Zn^{2+} ions and O^{2-} hosts, which are known to hinder Zn^{2+} diffusion, were effectively reduced by the unique π-conjugated structure of PANI. Differential charge density was then calculated for both pristine V_2O_5 (Figure 5B) and PANI-V_2O_5 (Figure 5C) as a single Zn^{2+} was inserted into the frameworks. Substantial charge depletion and accumulation could be identified around Zn and adjacent O atoms, respectively. The charge redistribution patterns were very similar between Zn and the four adjacent O atoms for both systems. However, charge accumulation was observed around the next-nearest O atoms in bulk V_2O_5 (Figure 5B), indicating strong binding interaction of Zn and sluggish Zn^{2+} diffusion in the pristine V_2O_5. From Figure 5D, the calculated binding energy of Zn ion inserted in PANI-V_2O_5 was markedly lower than that in pristine V_2O_5 (1.67 vs 2.06 eV), suggesting that it was much easier for Zn ions (de)intercalation in PANI-V_2O_5. As a result, the PANI-intercalated V_2O_5 electrode exhibited a high rate capability of 197.1 mAh/g at the current density of 20 A/g with a capacity retention of 97.6% over 2000 cycles. Similarly, Zhang *et al.*[79] fabricated a cathode structure with PANI in situ intercalated into layered vanadium oxide in order to enlarge the lamellar spacing and enhance the battery performance. As shown in Figure 5E, the in-situ XRD results revealed that the crystal structure of PANI100–V_2O_5 is fully reversible during the intercalation and extraction of Zn^{2+} ions. More importantly, the accumulation of more Zn^{2+} ions can be achieved via the enlarged interlayer spacing from 1.42 to 1.62 nm, as calculated from the variation of diffraction peaks, leading to a larger specific capacity. The in-situ characterizations in this work demonstrated that PANI as the guest materials not only enlarged the lattice spacing for ready accumulation of Zn^{2+} ions and improved the specific capacity, but also buffered the volumetric expansion and improved the stability due to the flexible molecular nature.

Furthermore, Mutlin *et al.*[80] found that intercalation of PANI into vanadium oxygen hydrate (VOH) led to not only an enlarged interlayer spacing, but also exfoliation of the VOH sheets, and hence the formation of a graphene-like nanosheet morphology. The obtained PANI–VOH nanosheets possessed a greatly boosted total charge storage capacity, due to abundant surface sites for reversible V^{5+} to V^{3+} redox reactions. Electrochemical impedance spectroscopy (EIS) and GITT analyses showed that with the PANI–VOH nanosheets, the charge-transfer resistance (R_{CT}) decreased and concurrently the diffusion coefficient of Zn^{2+} increased (by a factor of 10~100), as compared to the VOH baseline. Besides PANI, polypyrrole (PPy) has also been used as intercalation pillars. Srinivasan *et al.*[81] studied the effect of PPy intercalation on the layered $VOPO_4$ host, and observed that the enlarged interlayer space made Zn^{2+} cation (de)intercalation feasible, leading to a high capacity and long cycle life. Moreover, Xia *et al.*[77] prepared poly(3,4-ethylenedioxythiophene) (PEDOT) intercalated $NH_4V_3O_8$ (PEDOT-NVO) as a cathode material, leading to an increased interlayer spacing of 10.8 Å (from 7.8 Å for pristine NVO). This cathode material exhibited an improved capacity of 356.8 mAh/g at 0.05 A/g and 163.6 mAh/g, even at the highest current density of 10 A/g (with a high retention from 0.05 to 10 A/g), and featured an ultra-long lifetime of over 5,000 charge-discharge cycles with a capacity retention of 94.1%. Additionally, Sun *et al.*[82] demonstrated that the introduction of PEDOT contributed to the formation of oxygen vacancy in V_2O_5, and meanwhile led to an enlarged interlayer spacing. The as-prepared cathode materials exhibited a high capacity of 449 mAh/g at a current density of 0.2 A/g, with an excellent cyclic performance of 94.3% after 6,000 cycles.

From these studies, one can see that intercalation of select polymers into host cathodes can not only enlarge the interlayer spacing, but also weaken the electrical interactions between Zn ions and host materials, and hence significantly improve the Zn^{2+} diffusion kinetics. To optimize the performance, further studies should be extended to the wide variety of other conducting polymers, along with the development of suitable fabrication methods. Additionally, the effects of electrolyte on the polymers should be taken into consideration for cathode design.

4.1.3 | Water intercalation

Water intercalation includes structural water molecules in host materials and intercalated water occurring during the charge/discharge process in aqueous ZIBs, where water molecules are co-intercalated with Zn ions upon discharge. Mai's group[83] has recently discussed the impacts of water on the electrochemical performance of ZIBs, where the water molecules could affect the electrode, active material, electrolyte, and the overall battery performance of ZIBs from different aspects.

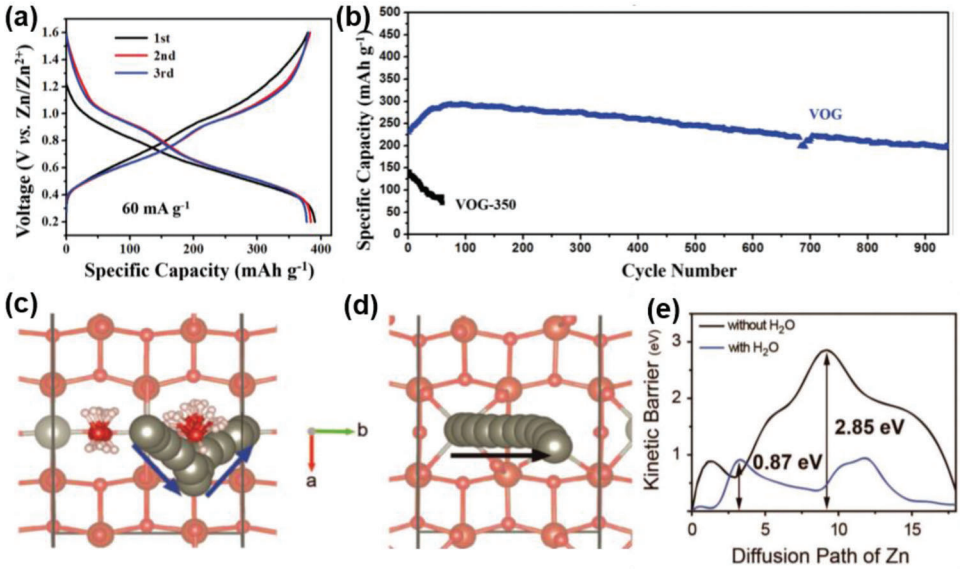

FIGURE 6 (A) Charge–discharge curves for the first three cycles of the as-prepared VOG. (B) Cycling performance of VOG and VOG-350 (without structural water) at 6 A/g (reproduced with permission from ref. [84]; copyright 2017, Wiley-VCH). Diffusion paths of Zn ion in V_6O_{13} (C) with and (D) without water (projected down [001]). (E) Calculated diffusion barriers for paths in (C) and (D) (reproduced with permission from ref. [67]; copyright 2019, Wiley-VCH)

In terms of the cathode materials, optimization strategies have been developed by exploiting the influence of water molecules on the crystal structure, type of compound bond, electronic structure, and valence state. Mai *et al.*[84] found that structural water molecules acted as "lubricants" and facilitated the reversible mobility of Zn^{2+} into the layered $V_2O_5{\cdot}nH_2O$/graphene structure (VOG), consequently leading to the high capacity of 381 mAh/g at 60 mA/g (Figure 6A) and outstanding cycling stability with a capacity retention of 71% after 900 cycles (Figure 6B). Furthermore, the interlayer water could act as an electrostatic shield to modulate the polarization effects, especially in multivalent ion batteries. The wide application of layered vanadates in ZIBs, such as $V_6O_{13}{\cdot}nH_2O$,[85] $Na_2V_6O_{16}{\cdot}3H_2O$,[86] $V_{10}O_{24}{\cdot}12H_2O$,[87] and $H_2V_3O_8$,[88] indicate the great potential of layered vanadium oxides containing structural water as ZIB cathode materials.

Moreover, upon discharge, water usually co-intercalates with Zn ions into the cathode materials in aqueous electrolytes. For instance, H_2O in the aqueous electrolyte can buffer the large charge density of divalent Zn^{2+} and enhance Zn diffusion, which endows the anhydrous V_2O_5 electrode with a high ion-diffusion coefficient of 10^{-10}-10^{-11} cm^2 s^{-1}.[89] Choi *et al.* [67] demonstrated that the water co-intercalation mechanism facilitated Zn ion diffusion throughout the host lattice and electrode-electrolyte interface via electrostatic shielding and concurrent structural stabilization. Based on the simulation results of water co-intercalation (Figure 6C), it was observed that Zn preferred to follow a zigzag route along the b axis from one octahedral site to the adjacent one, with water molecules rearranged to minimize electrostatic repulsion from the lattice oxygen atoms. In the anhydrous case (Figure 6D), although Zn ion diffusion took a more straightforward path, it tended to skew toward one side at the end. As shown in Figure 6E, the kinetic barrier for Zn ion diffusion for the case with water was much lower than that without water, demonstrating easier diffusion of Zn ions in the cathode materials with the assistance of water.[67] Therefore, water co-intercalation provides a low kinetic energy barrier by expanding the cross-sectional area along the diffusion path and lowering the charge of Zn, and the combined effects may contribute to the high-rate performance.

Similar to metal ions and polymers, either structural water or intercalated water can act as effective pillars to improve the structural stability of cathode materials during the charge/discharge processes, as well as provide fast Zn^{2+} diffusion paths. More importantly, water can be used as a "lubricant" to lower the Zn^{2+} migration energy barrier and thus facilitate Zn^{2+} diffusion. To further improve the performance, co-intercalation of multiple pillars into cathode materials can be conducted to exploit their synergistic interactions. Yet, it remains a challenge to optimize the loading ratios of the various pillars in the cathode materials for maximal performance.

4.2 | Heteroatom doping

Heteroatom doping can effectively modify the structure of the cathode materials, such as tuning the electronic structure, enhancing the electrical conductivity, and facilitating ion diffusion, all conducive to performance

doi.org/10.1002/elsa.202100090

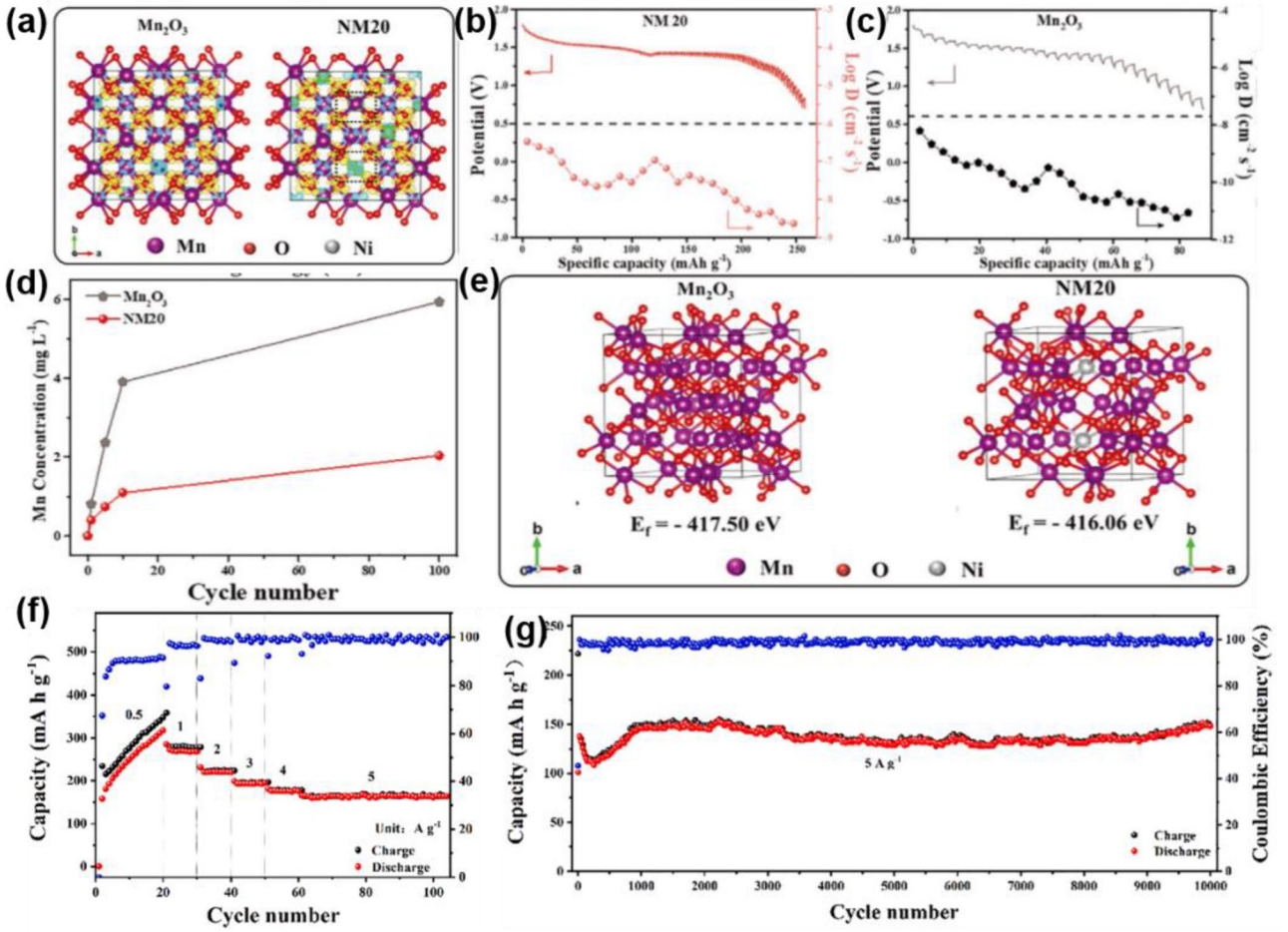

FIGURE 7 (A) Charge distribution of Mn_2O_3 and NM20. GITT profiles and diffusion coefficients of (B) NM20 and (C) Mn_2O_3. (D) ICP measurement of manganese dissolution in 2 m $ZnSO_4$ electrolyte after different cycles. (E) Calculated formation energy (in eV) of Mn_2O_3 and NM20 (reproduced with permission from ref. [23]; copyright 2020, Wiley-VCH). (F) Rate performance of MZO at various current densities from 0.5 to 5 A/g. (G) Cycle performance and Coulombic efficiency of MZO at a current density of 5 A/g (reproduced with permission from ref. [91]; copyright 2021, Elsevier)

improvement. There are generally two types of dopants, metal ions, and nonmetal atoms.

Metal-ion dopants are expected to optimize the electronic state and stabilize the structure of the host materials, consequently addressing the issues of dissolution during the cycling process, low electrical conductivity, and structural degradation of cathodes during charge/discharge. Huang *et al.* [23] prepared a Ni-doped Mn_2O_3 (NM) to suppress the dissolution of manganese. The incorporation of Ni^{2+} was found to promote electronic rearrangement, enhance electrical conductivity, and improve the reaction kinetics and electrochemical performance. Moreover, the extra electrons in NM with an atomic ratio of Ni and Mn in the precursor of 1:20 (NM20) were accumulated around the Mn atoms adjacent to the inserted Ni atoms (Figure 7A), which generated a strong interaction between the interconnected manganese and oxygen atoms (Mn-O), thus enhancing its structural stability. As shown in Figure 7B, the Zn ion diffusion coefficient ($D_{Zn}{}^{2+}$) of NM20 during discharging was estimated to be 10^{-7}–10^{-9} cm^2/s, about 10–10^2 times higher than that of Mn_2O_3 (Figure 7C), indicating enhanced diffusion in NM20. Moreover, the evolution of manganese concentration in the electrolyte was detected via the inductively coupled plasma (ICP) measurement and the results were displayed in Figure 7D. The dissolution of manganese could be effectively alleviated to only 2 mg/L with the NM cathodes; in sharp contrast, the manganese in pure Mn_2O_3 displayed a fast dissolution in the first few cycles. The suppression of manganese dissolution originated from stabilizing the Mn-O bond of Mn_2O_3 by reducing the formation energy (from 417.5 to 416.1 eV) after Ni^{2+} steadily intercalated into Mn_2O_3 (Figure 7E), which effectively strengthened the inherent stability. In another study,[90] Wang *et al.* loaded nickel and cobalt co-substituted spinel $ZnMn_2O_4$ nanoparticles homogeneously onto N-doped reduced graphene oxide ($ZnNi_xCo_yMn_{2-x-y}O_4$@N-rGO), and observed that the co-substituting of nickel and cobalt effectively facilitated Zn^{2+} de-intercalation and stabilized the spinel structure that productively prevented the Jahn-Teller distortion of Mn^{3+}.

Mn has also been used to dope ZnO as a high-performance cathode, which not only adjusts the electronic structure, but also enhances the electrical conductivity, thereby upraising the reaction kinetics.[91] Consequently, the Mn-doped ZnO cathode (MZO) displays an appreciable rate performance, with a capacity of 268.1 mAh/g at 1 A/g, and retains 163.8 mAh/g at 5 A/g (Figure 7F). Most importantly, a high energy density (206.9 Wh/kg), power density (6896.7 W/kg), and superior cycle durability (146.7% after 10,000 cycles relative to the first cycle, Figure 7G) endow this material with a high potential for energy storage.

Other ions, such as Al, and Ag,[92,93] have also been used as dopants to productively tune the electrochemical properties of cathode materials, leading to significantly improved energy density, rate capability, and cyclic stability.

Doped host materials with nonmetal atoms, such as N, O, P, and S, represent another promising route to improve the electrochemical properties.[94,95] In ZIBs, nonmetal atom-doped carbons have attracted extensive attention as both conductive substrate and modification coating for active materials to improve the electrical conductivity and alleviate volumetric change of the cathodes. For instance, N-doped graphene has been used to support $ZnMn_2O_4$ nanoparticles, forming high-performance nanocomposite cathodes for ZIBs.[44] These cathodes with ultrafine $ZnMn_2O_4$ nanoparticles anchored on N-doped graphene exhibit an ultralong cycle life with 97.4% capacity retention after 2,500 cycles at 1000 mA/g, which is attributed to the synergistic effect of superfine $ZnMn_2O_4$ nanoparticles that provide rapid surface capacitive reaction and short electron/ion transport path lengths, as well as the highly conductive N-doped graphene medium that facilities fast electron transport and stabilizes the composite structure to tolerate volume expansion during charge/discharge. Moreover, N-doped hollow carbon spheres (NHCSs) have been employed as growth substrates to effectively promote the uniform distribution of active MnO_2 nanosheets, increase the total contact area at the electrode-electrolyte interface, and facilitate exposure of active sites for maximum utilization of the active materials.[96] The combination of NHCSs also significantly enhances the conductivity of the positive electrode. Meanwhile, the MnO_2-NHCSs hybrid with a hollow structure possesses a large specific surface area, a large cavity volume, and a short ion diffusion path, which is kinetically favorable for ion and electron transport.

Besides being used as the substrates for active material support, doped carbons can also act as a modification layer for cathode materials. Sun *et al.* [97] prepared an onion-like N-doped carbon modified MnO_x nanorod (MnO_x@N-C) as cathode, which exhibited a high capacity of 305 mAh/g after 600 cycles at 500 mA/g and retained a capacity of 100 mAh/g at 2000 mA/g after long-term cycling of up to 1600 cycles. The outstanding electrochemical performance was attributed to the amorphous carbon shell and the onion-like N-doped carbon derived from the carbonization of ZIF-8 in such hybrid structures, which significantly enhanced the overall electrical conductivity and facilitated effective electron transport. In a recent study,[98] a hybrid structure consisting of Mn-doped V_6O_{13} nanoribbons and N-S modified porous carbon structure (MnVO/(SN)-C) was fabricated, where the doping of Mn ion into V_6O_{13} was found to optimize the electronic structure, and the rigid and conductive N-S doped carbon structure boosted the electron transport rate in electrochemical reactions, and suppressed the huge volume expansion. As a result, this electrode exhibited a high capacity of 414.2 mAh/g, high rate capability (with a 67.37% capacity retention from 1 to 10 A/g), and outstanding long-term cycle stability (100.1% after 1000 cycles at 10 A/g).

Doping is expected to apply to a wide range of cathode materials of ZIBs, in comparison with the interlayer intercalation method that is only available for layered materials. Notably, doping is not limited to active materials. It can also be applied to the substrates and coating materials in the composite cathodes. Upon doping modification, the intrinsic properties (electrical conductivity, structure stability, etc) of the cathode materials can be significantly enhanced, due to manipulation of the electronic structure and even the phase transformation path. Furthermore, doping can lead to an imbalanced charge distribution and local electric field inside the crystal structure of the cathode materials, thus boosting their ion/electron migration rates. Yet, currently most research mainly focuses on the choice of dopants and their synthesis methods, whereas the doping mechanism and the effects of dopant concentration and occupation position have been rarely reported. Further studies are desired to address these important issues.

4.3 | Defect engineering

Defect engineering has been recognized as an essential way to modify the electronic properties of materials, in particular, cathode materials for ZIBs. Typically, there are four types of material defects,[99,100] (1) oxygen vacancy, (2) cation vacancy, (3) cationic doping, and (4) anionic doping. Since doping has been discussed in the previous section, this section mainly focuses on the oxygen and cation vacancies.

4.3.1 | Oxygen vacancy

Due to the low formation energy, oxygen vacancy has been considered as a major defect to tune the electronic structure and physicochemical properties of cathode materials. Xia *et al.*[101] developed a low-temperature defect

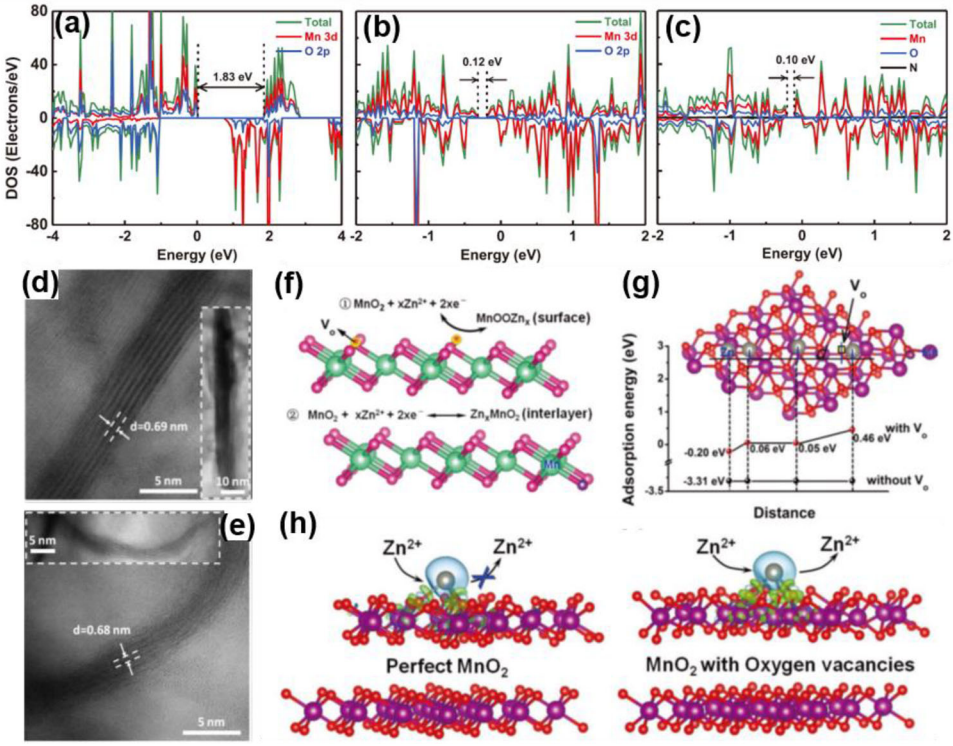

FIGURE 8 DOS of (A) MnO_2, (B) MnO_{2-x}, and (C) N-MnO_{2-x} (reproduced with permission from ref. [101]; copyright 2019, Wiley-VCH). (D) Atomically resolved scanning transmission electron microscopy-annular bright-field (STEM-ABF) image of a C-MnO_2 nanosheet, with a larger view of the straight nanosheet in the inset. (E) Atomically resolved STEM-ABF image of one curved Od-MnO_2 nanosheet, with a larger view of the nanosheet in the inset. (F) Schematic illustration of oxygen-deficient σ-MnO_2 for Zn ion storage. (G) Calculated adsorption energies for Zn^{2+} on the surfaces of pristine and oxygen-deficient σ-MnO_2. Four possible sites for Zn adsorption are selected with a different distance from oxygen vacancy (VO). (h) Schematic illustration of Zn^{2+} adsorption/desorption on pristine and oxygen-deficient MnO_2 (reproduced with permission from ref. [99]; copyright 2019, Wiley-VCH)

engineering method to fabricate N-doped MnO_2 cathode with abundant oxygen vacancies. The N dopants and oxygen vacancies in MnO_2 were confirmed by synchrotron spectroscopy measurements, and density functional theory (DFT) calculations were conducted to investigate the effects of N dopants and oxygen vacancies on the electron densities and electrochemical properties of MnO_2. As shown in Figure 8a-8b, MnO_{2-x} (0.12 eV) exhibited a much lower bandgap than pristine MnO_2 (1.83 eV), indicating that the formation of oxygen vacancies could greatly improve the electrical conductivity. After N doping, the bandgap of N-MnO_{2-x} further decreased to 0.1 eV (Figure 8C), which further enhanced the electrical conductivity. In another study,[99] Xue *et al.* optimized the electrochemical performance of MnO_2 cathode materials by the formation of oxygen vacancies (O_d-MnO_2). As compared to pristine MnO_2 that possessed an interlayer spacing of ca. 0.69 nm (Figure 8D), the O_d-MnO_2 nanosheets exhibited a slightly shorter interlayer spacing of ca. 0.68 nm and were mostly curved, thinner, and shorter (Figure 8E). Notably, Zn^{2+} storage in σ-MnO_2 arose from diffusive and capacitive contributions (Figure 8F). From Figure 8G, one can see that the Gibbs free energies ($\Delta G_{Zn^{2+}}$) of Zn^{2+} adsorption were close to the thermoneutral value of ca. 0.05 eV at the vicinity sites to oxygen vacancy in O_d-MnO_2, which was energetically conducive to reversible Zn^{2+} adsorption/desorption; by contrast, $\Delta G_{Zn^{2+}}$ became markedly more negative at ca. −3.31 eV on pristine MnO_2, indicating much stronger adsorption of Zn^{2+}. This would render desorption difficult, mask the electrochemically active surface area (Figure 8H), and eventually compromise the capacity performance.

Oxygen vacancy has also been exploited for performance enhancement in V-based oxides. Peng *et al.*[102] prepared oxygen-deficient V_6O_{13} (O_d-VO) to increase divalent cation-intercalating sites and thereby the capacity. The O_d-VO structure showed a thermoneutral Gibbs free energy of Zn^{2+} desorption, which suggests an effortless Zn^{2+} release by the cathode in its discharge state, fully accessible for the next charging process. In contrast, pristine VO (p-VO) exhibited a much higher Gibbs free energy of desorption, again, indicating a difficult Zn^{2+} release, thus leading to a deterioration in cycling stability. As shown in Figure 9A, the average diffusion coefficient of Zn^{2+} ($D_{Zn^{2+}}$) in O_d-VO at the discharge and charge plateaus were approximately 1.1×10^{-11} and 0.4×10^{-11} cm^2/s, respectively, which are

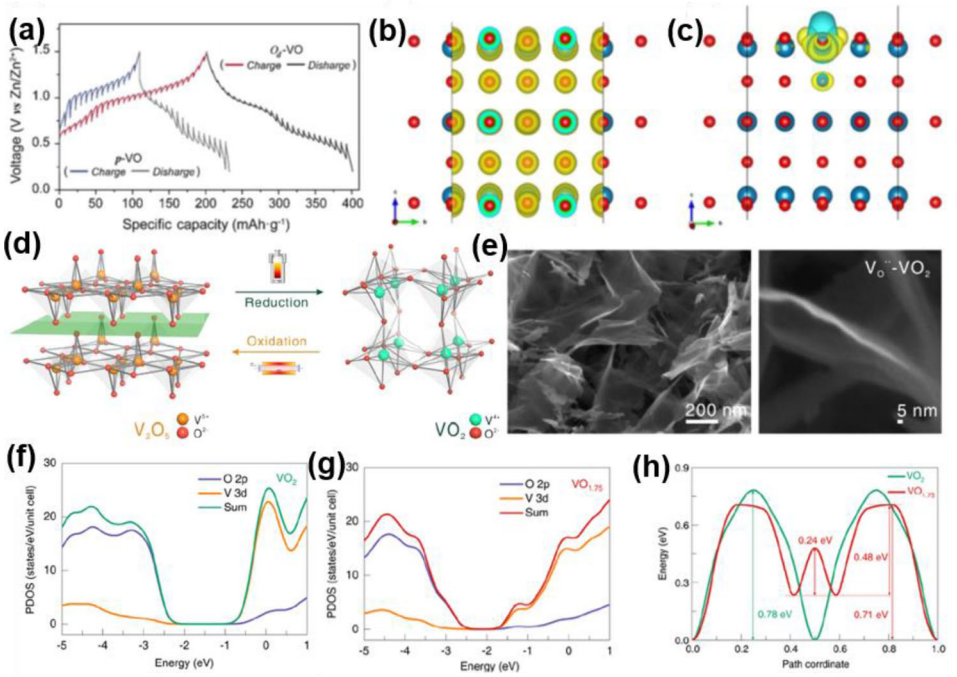

FIGURE 9 (A) GITT profiles of p-VO and O_d-VO electrodes, and the corresponding charge distribution of (B) p-VO and (C) O_d-VO (reproduced with permission from ref. [102]; copyright 2019, Wiley-VCH). (D) Schematic illustration of the synthesis process of $V_O^{\bullet\bullet}$–VO_2. (E) SEM images of $V_O^{\bullet\bullet}$–VO_2. Projected density of states (PDOS) of (F) VO_2 and (G) $VO_{1.75}$. (H) Calculated Zn ion diffusion energy barriers in VO_2 and $VO_{1.75}$ (reproduced with permission from ref. [103]; copyright 2020, American Chemical Society)

comparable to that of Li^+ and much higher than that of p-VO. Additionally, p-VO exhibited a uniform charge distribution (Figure 9B), while electrons were accumulated around O_d-VO (Figure 9C). These observations indicate that when the oxygen atoms are extracted from the vanadium oxide lattice, defective sites form with spare electrons, which can then contribute to the delocalized electron cloud of O_d-VO, leading to an increased capacity.

Furthermore, Cao *et al.* [103] introduced oxygen vacancy into VO_2 ($V_O^{\bullet\bullet}$–VO_2) through a repeated phase transition process (Figure 9D) and systematically investigated the impacts of oxygen vacancy on Zn^{2+} intercalation in VO_2. The obtained $V_O^{\bullet\bullet}$–VO_2 exhibited a nanosheet morphology with a thickness of ca. 5 nm (Figure 9E), and the $VO_{1.75}$ model was chosen for first-principles calculations to study the impacts of $V_O^{\bullet\bullet}$ on their electronic structures and zinc ion storage, primarily because of a similar $V_O^{\bullet\bullet}$ concentration. Figure 9F and G shows the DOS and band structure of the $VO_{1.75}$ and VO_2 structures. After the introduction of $V_O^{\bullet\bullet}$, $VO_{1.75}$ exhibited a narrower bandgap and a lower diffusion energy barrier (0.24–0.71 eV) than VO_2 (0.78 eV) when zinc ions passed through the oxygen vacancy sites (Figure 9H). This would enable fast zinc ion diffusion along the b tunnel in the host lattice.

The oxygen-vacancy strategies are the most commonly used method for structural engineering of cathode materials, due to the easy formation of oxygen vacancy during sample preparation. Various fabrication methods have been employed, such as hydrothermal/solvothermal process, chemical etching, electrochemical treatment, etc., which show great potential in cost-effective, large-scale industrial applications. However, it is difficult to control the precise location and concentration of oxygen vacancy in the cathode materials. In addition, advanced characterization techniques are needed to investigate the influences of oxygen vacancy on the Zn ion diffusion process.

4.3.2 | Cation vacancy

Cation vacancy refers to a cation missing from its lattice site, and this type of defect usually occurs in compounds where metals can exhibit a variable valency, such as Mn-based oxides. Chen's group first developed a cation-deficient spinel $ZnMn_2O_4$ cathode for ZIBs.[22] In a perfect spinel without cation deficiency, Zn^{2+} ions migrate from one tetrahedral site (4a) to another by passing through an unoccupied octahedral site (8c) and thus experience a strong electrostatic repulsion from Mn cations in a neighboring octahedral site (8d) (Figure 10A), which significantly hinders Zn^{2+} diffusion. For comparison, the Mn-vacancy-rich structure allows for easy Zn-ion diffusion with a weakened electrostatic barrier, leading to the high mobility of Zn^{2+} cations and consequently fast reaction kinetics (Figure 10A). As a result, cation-defected $ZnMn_2O_4$ exhibits a reversible specific capacity of

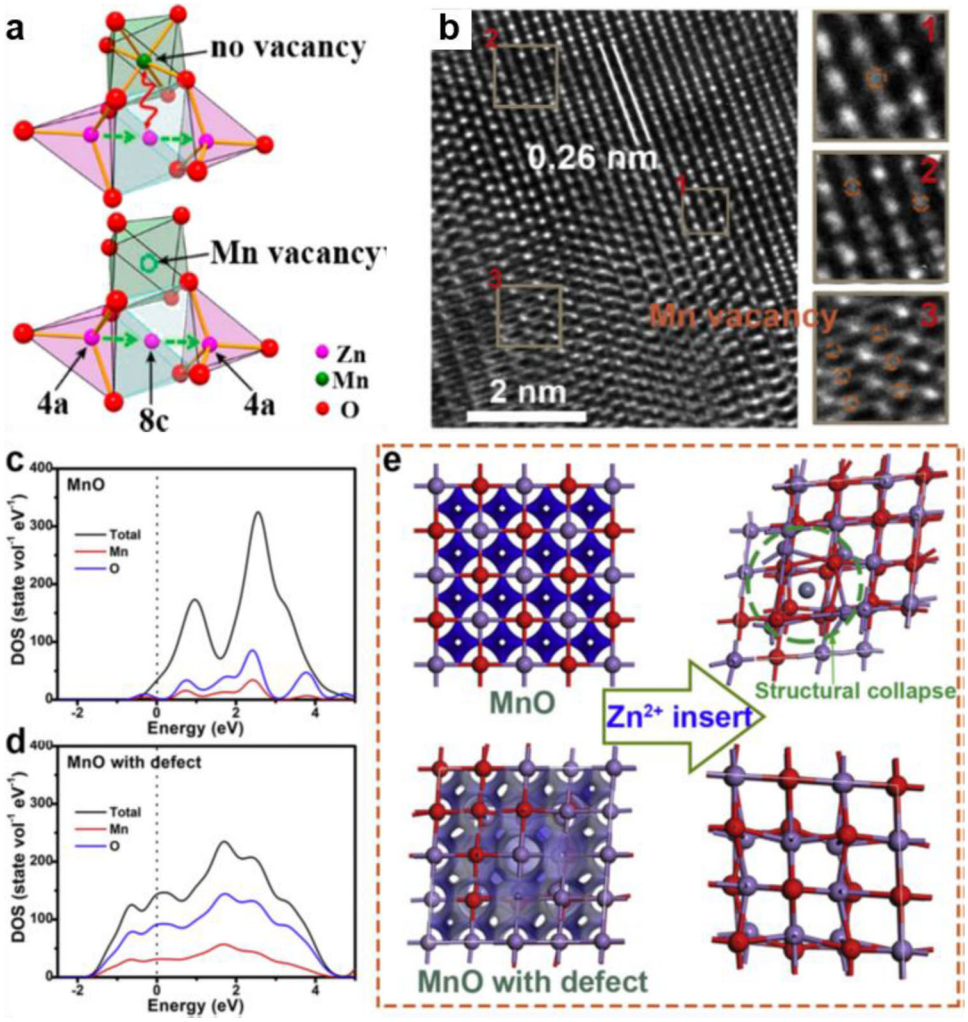

FIGURE 10 (A) Proposed Zn^{2+} diffusion pathway in ZMO spinel without and with Mn vacancies (reproduced with permission from ref. [22]; copyright 2016, American Chemical Society). (B) HRTEM of the first fully charged state of MnO. The orange circles highlight the missing Mn column position, indicating the formation of Mn cation defects. The right panels are the magnified images from the areas marked by brown squares. Calculated DOS of (C) pristine MnO and (D) MnO with Mn defects. (E) Charge distribution of pristine MnO and MnO with Mn defects, and the structures after Zn ion insertion. The green circle shows structural collapse (reproduced with permission from ref. [104]; copyright 2020, Elsevier)

150 mAh/g at 50 mA/g and a high capacity-retention of 94% after 500 cycles at a high current density of 500 mA/g. Additionally, Zhou *et al.* [104] developed an in situ electrochemical approach to activate MnO by inducing Mn defects, which were formed through a charge process, and the introduction of Mn defects significantly enhanced the electrochemical activity of MnO for aqueous ZIBs. High-resolution transmission electron microscopy (HRTEM) study (Figure 10B) showed a basic structure of MnO with an interplanar spacing of 0.26 nm, corresponding to the (111) plane of MnO. The magnified images (areas 1, 2, and 3) clearly showed that the Mn columns in some areas became weak or missing, indicating the formation of Mn defects (marked with dotted circles) in MnO. From the calculated DOS of MnO with and without Mn defects (Figure 10C and D), one can see that the formation of Mn defects in MnO increased the charge density around the Fermi level, leading to enhanced electrical conductivity, as compared to pristine MnO. As shown in Figure 10E, the structure of pristine MnO was greatly damaged upon Zn^{2+} insertion, whereas no obvious structural change was observed with Mn-defect MnO, as the Mn defects created large insertion channels and available active sites for Zn^{2+} ions, enabling fast reaction kinetics.

In essence, cation vacancy can help improve ion diffusion kinetics and increase electrochemical active sites for energy storage of the cathode materials. However, compared to oxygen vacancy, cation-vacancy engineering has been mostly confined to Mn-based oxides for ZIBs. Further research is needed to extend the strategy to other cathode

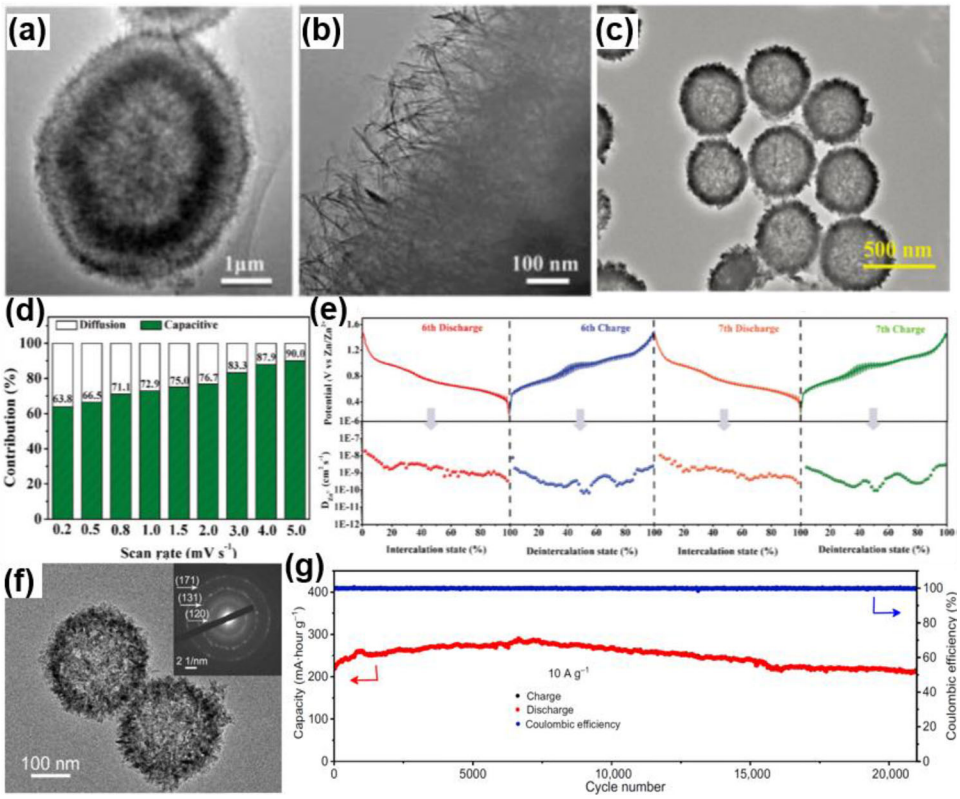

FIGURE 11 (A, B) Low-magnification TEM images of the obtained HAVO hollow microspheres (reproduced with permission from ref. [110]; copyright 2020, Elsevier). (C) TEM image of VO_2 hollow spheres. (D) Percentages of capacitive and diffusion contributions of VO_2 at different scan rates. (E) Charge/discharge curves and the corresponding D_{Zn}^{2+} values of the VO_2 electrode in the sixth and seventh cycles (reproduced with permission from ref. [111]; copyright 2019, Royal Society of Chemistry). (F) TEM image and selected area electron diffraction patterns (inset) of VOOH. (G) Long-term cycling performance of Zn//ZVO battery at 10 A/g (reproduced with permission from ref. [112]; copyright 2019, American Association for the Advancement of Science)

materials, and to exploit the synergistic interactions of various types of defects for more complicated structural engineering.

4.4 | Micro/nanostructure design

Design and construction of micro/nanostructures is another promising strategy to improve the electrochemical performance of cathode materials, due to the enlarged specific surface area, enhanced accessibility to electrolyte, as well as increased active sites for ion absorption.[105,106] In fact, cathode materials with micro/nanospheres, nanosheets, nanofibers, and nanotubes have been widely used for ZIB applications,[107–109] demonstrating the significance of micro/nanostructure design in the optimization of electrochemical performance for cathode materials. In this section, two types of micro/nanostructure designs (hollow and core-shell structures) of cathodes will be examined to reveal the unique ion/charge transport mechanisms in such structures.

4.4.1 | Hollow structure

Cathode materials with a hollow structure (i.e., a thin shell and high active surface area) are anticipated to facilitate ion transport between layers, improve ion adsorption, and enhance surface redox reactions. Additionally, hollow nanostructures offer a large void space, which significantly alleviates the volume change of cathodes during charge/discharge. For instance, Wang *et al.*[110] prepared $H_{11}Al_2V_6O_{23.2}$ (HAVO) hollow spheres as cathode materials for ZIBs, which were composed of nanosheets with an average thickness < 5 nm (Figure 11A) and found to serve as effective channels for ions transport and electrolyte wetting (Figure 11B). In another study,[111] vanadium dioxide (VO_2) hollow nanospheres were employed as cathode materials for ZIBs (Figure 11C), which delivered a high reversible discharge capacity of 408 mAh/g at 0.1 A/g, an exceptional rate performance of 200 mAh/g at 20 A/g, and long cyclic stability (with a low capacity-fading rate of 0.0023% per cycle over 30,000 cycles). Moreover, the bar chart in Figure 11D clearly shows the capacitive

Review
doi.org/10.1002/elsa.202100090
Chemistry Europe
European Chemical Societies Publishing

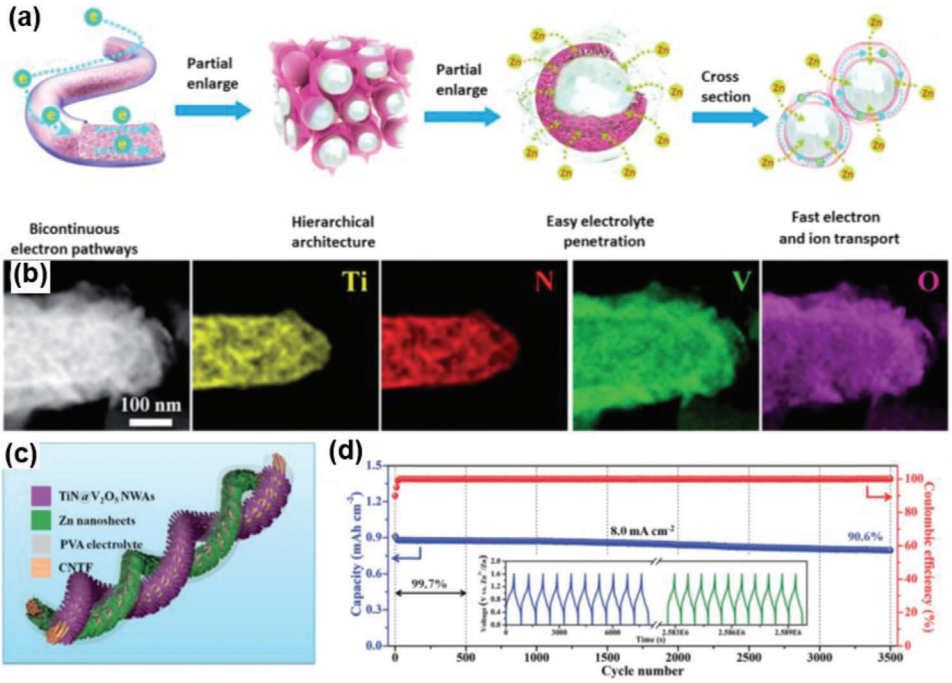

FIGURE 12 (A) Scheme of the energy storage process in one-dimensional core-shell structures (reproduced with permission from ref. [24]; copyright 2019, American Chemical Society). (B) TEM image and EDS elemental maps of Ti, N, V, and O of a single TiN@V_2O_5 nanowire core-shell nanocomposite. (C) Schematic illustration of a fiber-shaped all-solid-state TiN@V_2O_5 NWA//Zn battery. (D) Long-term cycling performance at 8.0 mA/cm^2. The inset displays the charge/discharge curves for the first and last 10 cycles (reproduced with permission from ref. [113]; copyright 2019, Royal Society of Chemistry)

contributions in energy storage of such cathode materials at different scan rates. With the sweep rate increased from 0.2 to 5.0 mV/s, the percentage of capacitive contribution grew from 63.8% to 90.0%, suggesting that the surface pseudocapacitance effect played a dominant role at high rates, which was favored for high-rate performance. Figure 11E shows the charge/discharge curves and the corresponding D_{Zn}^{2+} values of the VO_2 electrode in the 6th and 7th cycles. It can be seen that the D_{Zn}^{2+} values during the two insertion and extraction processes are on the order of 10^{-8} to 10^{-10} cm^2/s, significantly higher than those reported previously.[111] The excellent electrochemical performance was ascribed to the interior hollow architecture that featured a large specific surface area, large internal cavity, permeable porous thin shells, and hence numerous reactive sites for guest ion insertion. This allowed facile infiltration of the electrolyte and facilitated rapid diffusion of Zn^{2+}. Zheng's group[112] used VOOH hollow nanospheres (Figure 11F) as precursors to fabricate porous Zn-vanadium oxide materials through electrochemical cycling. The obtained $Zn_{0.3}V_2O_5{\cdot}1.5H_2O$ (ZVO) cathode delivered a high specific capacity of 426 mAh/g at 0.2 A/g and exhibited an unprecedented long-term cyclic stability with a capacity retention of 96% over 20,000 cycles at 10 A/g (Figure 11G).

Hollow nanostructures demonstrate great potential for ZIB applications with abundant Zn ion storage sites, short transport pathways, and sufficient space to buffer the volume changes during the intercalation/de-intercalation of Zn ions. Nevertheless, their low volumetric energy density is the main obstacle for practical applications. Thus, striking a balance between the rate/cycling performance and volumetric energy density is the key in battery research, where a good control of the hollow structure with a precise shell thickness and well-defined morphology will be a focus in future research.

4.4.2 | Core-shell structure

Core-shell structures usually possess superb chemical and physical properties, as compared to their single-component counterparts, due to synergistic effects between the different components. Zhang *et al.*[24] prepared fiber structures based on a metal oxide core and a carbon shell. Specifically, $Zn_2V_2O_7$ and V_2O_5 were employed as the cores, which were then coated with a carbon layer. As shown in Figure 12A, such one-dimensional core-shell structures provided bi-continuous conductive pathways and highly porous networks for supporting the in situ formed metal oxide nanoparticles, thus facilitating fast electron/ion transport and high mass loading. Yao *et al.* [113] fabricated a TiN@V_2O_5 core-shell heterostructure with V_2O_5 nanosheets anchored on TiN nanowire arrays for ZIBs (Figure 12B). The TiN@V_2O_5 cathode

exhibited a remarkable Zn-ion storage performance, with a high capacity of 1.45 mAh/cm^2 (636.0 mAh/g) at 0.5 mA/cm^2 and a high rate capability of 1.11 mAh/cm^2 (486.8 mAh/g) at 10 mA/cm^2. The outstanding electrochemical performance was attributed to the introduction of TiN nanowire arrays as the 3D conductive skeleton, and secondary-growth substrate increased the mass loading of the V_2O_5 nanosheets and provided rapid transfer of ion and charge, further improving the capacity, rate performance, and cycling stability. Consequently, flexible wire ZIB was assembled through such TiN@V_2O_5 core-shell fibers as cathode and Zn nanosheets grown on CNT fibers as anode (Figure 12C), and showed a high energy density and excellent cyclic stability with a capacity retention of over 90% after 3500 cycles (Figure 12D).

Cathode materials with a core-shell hierarchical structure are expected to exhibit outstanding electrochemical performance, due to the synergistic effect between the core and shell parts. However, it is difficult to precisely control the structural parameters, such as the diameter, length, and thickness of the core or shell. Moreover, the formation mechanism remains largely elusive, and the fabrication technology has not yet matured, limiting their industrial applications. Further research is urgently needed to address these issues.

4.5 | Composite construction

In order to further improve the electrochemical performance of cathode materials, composites with two or more components have been constructed by combining the advantages of each component in the structure and exploiting the synergistic effects between the different components. Mai *et al.* [114] have discussed the heterostructure composite electrodes for ZIBs. From the viewpoint of structural optimization, reconstruction of the electrode structure with the participation of functional materials is an effective method to improve the overall performance of ZIBs. For example, Niu *et al.* [115] fabricated a freestanding rGO/VO_2 electrode through a freeze-drying method. The cross-linked porous interconnected channels constructed by ultra-thin graphene films and nanostructured VO_2 provided a fast electron transfer for electrodes during the charge/discharge process. In sharp contrast, in the bare VO_2 cathode, electron transport was blocked by unconducive binders. The functional structural components can be either active or non-active materials.[116,117]

For composites that contain only electrochemically active materials for Zn ion storage, every component contributes to energy storage. Yang *et al.* [118] prepared a V_3O_7/V_2O_5 composite as the cathode for ZIBs and observed that the synergistic effects between V_3O_7 and V_2O_5 promoted the change of vanadium valence states from +5 (or +4) to +3 during redox reactions, and the electron transfer resulted in an increased capacity and improved cyclic stability, as compared to V_3O_7 or V_2O_5 alone. Qin *et al.* [119] designed V_2O_5/NaV_6O_{15} bi-phase composites as ZIB cathodes and found that the plentiful phase boundaries in the composites generated significant crystal defects as well as active sites, which were advantageous for Zn^{2+} storage and contributed to the pseudocapacitive effect; in addition, the bi-phase of V_2O_5/NaV_6O_{15} significantly enriched the redox reactions to buffer the stress during Zn^{2+} insertion. As a result, the V_2O_5/NaV_6O_{15} composite exhibited excellent long-term cycling stability, with a high capacity of 164 mAh/g after 2000 cycles at 5 A/g and 116.7 mAh/g after 4000 cycles at 10 A/g. Note that whereas an increasing number of active sites were formed in such composite cathodes, the interfacial resistance was increased significantly, and the poor bonding between different active phases might lead to structural collapse during the cycling process, consequently defeating their primary purpose as high-performance cathodes.

Carbon structures have been widely utilized as substrates to prepare composite cathodes of ZIBs in combination with other active materials,[120,121] such that the aggregation of the active materials can be minimized on the surface. Additionally, continuous conductive networks formed by carbon nanostructures can provide fast transfer channels for ions/electrons, enhancing the conductivity of the composite cathodes. Notably, carbon structures in some cases can act as a buffer layer to alleviate the volumetric change of cathode materials during the charge/discharge process. For example, carbon nanotubes (CNTs) have been employed to stitch zinc pyrovanadate ($Zn_3(OH)_2V_2O_7{\cdot}2H_2O$, CNT-stitched ZVO) nanosheets, forming high-performance wearable cathode materials for ZIBs.[122] With the CNT-stitched 2D nanosheets (Figure 13A), the open frameworks of ZVO provided a required spacing for reversible Zn^{2+} (de)intercalation, and the stitching CNTs offered the desperately needed electrical conductivity and mechanical robustness across the ZVO 2D nanosheets. More importantly, the nanosheet arrays possessed abundant two-dimensional ion channels in the exposed b−c planes, which were crucial to promote charge transfer and accelerate ion access at the electrode/electrolyte interface with a short Zn^{2+} and electron transportation path, whereas the stitching CNTs provided the desperately needed electrical conductivity across the ZVO nanosheets (inset to Figure 13A).[122] As a result, the fiber-shaped quasi-solid-state ZIB, assembled using such cathodes, demonstrated an ultrahigh rate capability, an impressive stack volumetric energy density of 71.6 mWh/cm^3 (Figure 13B), and outstanding cyclic stability.

Lu *et al.* [123] prepared MnO_2/graphene composite cathodes and observed significantly enhanced electrochemical properties. The graphene nanosheets-interconnected

Review
doi.org/10.1002/elsa.202100090
Chemistry Europe
European Chemical Societies Publishing

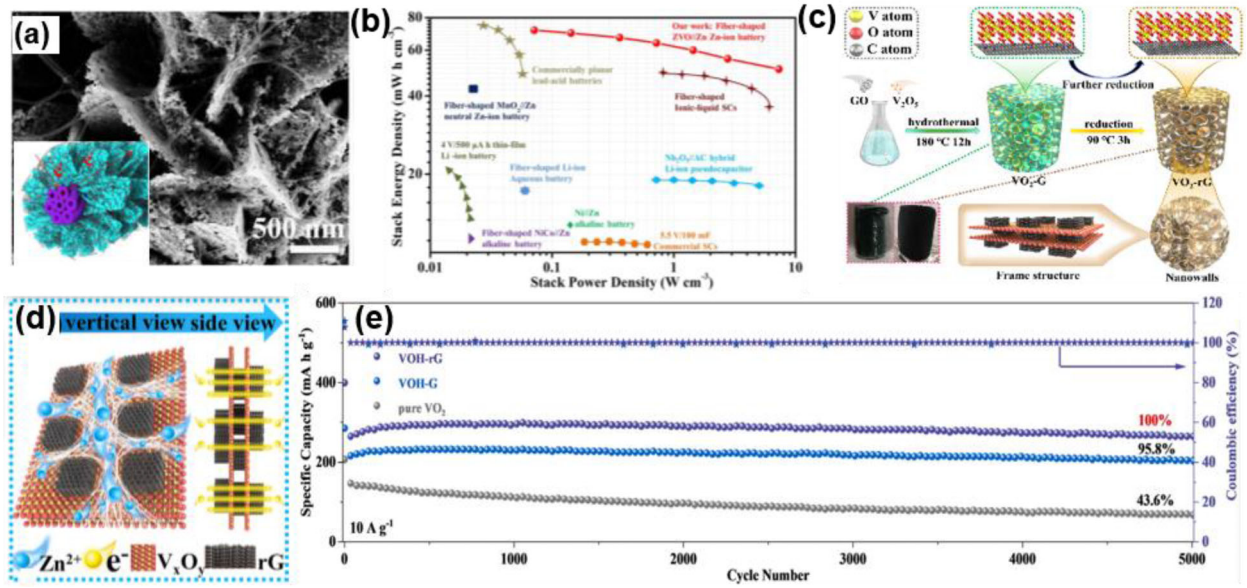

FIGURE 13 (A) SEM image of 3D CNT-stitched ZVO NSs@OCNT fiberss. Inset shows the schematic illustration of electron transfer in the CNT-stitched ZVO cathode. (B) Ragone plot to compare the energy storage performance of various devices (reproduced with permission from ref. [122]; copyright 2020, American Chemical Society). (C) Schematic illustration of the fabrication of 3D spongy VO_2-rG. (D) Schematic illustration of Zn ion/electron transfer in the architectural frame structure of VO_2-rG. (E) Long-term cycling of VO_2-rG at 10.0 A/g (reproduced with permission from ref. [25]; copyright 2021, Elsevier)

MnO_2 nanorods not only improved the conductivity of MnO_2 but also endowed the electrode with the ability to accommodate the structural damage and dissolution of MnO_2 during the charge/discharge process, leading to an enhanced rate and cyclic stability. Wang *et al.* [25] prepared a multifaceted $V_2O_5{\cdot}nH_2O$-graphene composite (VOH-rG) through an in-situ self-transformation process using three-dimensional spongy VO_2-graphene (VO_2-rG) as the precursor (Figure 13C). Benefiting from the highly conductive heterointerfaces, rich reaction sites, and numerous ion diffusion channels of VO_2-rG, almost 100% VO_2 nanobelts were converted into VOH during the first charging with few side reactions, indicating highly efficient transformation kinetics. Additionally, numerous graphene layers were anchored on the surface of the VO_2 nanobelts to construct an architectural frame structure (Figure 13C), acting as "corbeled pillars," which is favorable for minimizing the self-stacking of VO_2 nanobelts, facilitating the diffusion of electrolyte, and enhancing the across-interlayer electron transfer (Figure 13D).[25] Consequently, the VOH-rG cathode exhibited a high capacity of 466 mAh/g at 0.1 A/g, an excellent rate performance (190 mAh/g even at 20 A/g), and cycling stability with 100% capacity retention over 5000 cycles (Figure 13E).

Carbon modification has been regarded as the most widely used strategy in the structural engineering of cathode materials for ZIBs. However, carbon materials alone possess negligible storage for Zn ions, and thus the introduction of carbon structures can satisfy the energy density of composite cathodes. Thus, the balance between the conductivity and energy density should be taken into consideration in the design of carbon-based composite cathodes. Additionally, the interfaces between different phases in the composite structures would inevitably create barriers for ion/charge transfer, resulting in an increased interfacial resistance, which is a daunting challenge in the construction of composite cathodes for ZIBs.

4.6 | Other strategies

Surface coating of the cathode materials has also been used as an effective way to improve the electrochemical performance of cathodes, where a uniform and stable protecting layer is constructed on the surface of the electrode material. Typically, conductive carbon has been widely used as the coating layer to modify the cathode materials, due to its high conductivity and easy processing. For example, Kim *et al.* [124] prepared carbon-coated α-MnO_2 nanoparticles (α-MnO_2@C) as cathodes of aqueous ZIBs. The carbon coating not only improved the electrical conductivity, but also significantly enhanced the specific capacity and cycling performance of the α-MnO_2 electrode. Meanwhile, *Xu et al.* [125] prepared carbon-coated $ZnNi_{0.5}Mn_{0.5}CoO_4$ ($ZnNi_{0.5}Mn_{0.5}CoO_4$@C) as ZIB cathodes, where the carbon film served as a protective layer for the insertion and migration of electrons and ions, leading to improved structural stability of the cathode material and enhanced battery performance.

Table 1 summarizes the performances of a range of cathode materials modified through different strategies, in

TABLE 1 Summary of the electrochemical performance of typical ZIB cathodes modified through different strategies

Strategy	Structural engineering	Cathode materials	Capacity	Cyclic stability	Reference
Intercalation of pillars	enlarge layer spacing, stabilize material structure, and reduce electrostatic interactions	Zn_xMnO_2	1.746 F/cm^2 at 2 mA/cm^2	83.1% capacity retention (5,000 cycles at 15 mA/cm^2)	[63]
		Cu-V_2O_5 (CuVO)	359 mAh/g at 1 A/g	180 mAh/g (10,000 cycles at 10 A/g)	[69]
		$Li_xV_2O_5{\cdot}nH_2O$	407.6 mAh/g at 1 A/g	192 mAh/g (1,000 cycles at 10 A/g)	[72]
		PANI-MnO_2	298 mAh/g at 0.05 A/g	280 mAh/g (200 cycles at 0.2 A/g)	[21]
		PANI-V_2O_5	353.6 mAh/g at 0.1 A/g	280 mAh/g (100 cycles at 0.2 A/g)	[65]
		$V_2O_5{\cdot}nH_2O$/graphene	381 mAh/g at 0.06 A/g	71% (900 cycles at 6 A/g)	[84]
Heteroatom doping	promote electronic re-arrangement and enhance electrical conductivity	Ni-doped Mn_2O_3	252 mAh/g at 0.1 A/g	≈85.6% capacity retention (2,500 cycles at 1 A/g)	[23]
		Mn-doped ZnO	268.1 mAh/g at 1 A/g	147 mAh/g (10,000 cycles at 5 A/g)	[91]
		$ZnMn_2O_4$/N-doped graphene	221 mAh/g at 0.1 A/g	97.4% capacity retention (2,500 cycles at 1 A/g)	[44]
		MnO_x@N-C	305 mAh/g at 500 m A/g	100 mAh/g (1,600 cycles at 2 Ag^{-1})	[97]
Defect engineering	modify the electronic properties	O_d-MnO_2	345 mAh/g at 0.2 A/g	80% capacity retention (2,000 cycles at 5 A/g)	[99]
		$V_O{}^{\cdot\cdot}$–VO_2	375 mAh/g at 0.1 A/g	175 mAh/g (2,000 cycles at 5 A/g)	[103]
		Mn-defective MnO	300 mAh/g at 0.1 A/g	116 mAh/g (1,500 cycles at 1 A/g)	[104]
Micro/nanostructure design	enlarge specific surface area, enhance accessibility to electrolyte, and increase the number of active sites	$H_{11}Al_2V_6O_{23.2}$ hollow spheres	288.4 mAh/g at 0.1 A/g	88.6% capacity retention (7,000 cycles at 5 A/g)	[110]
		VO_2 hollow spheres	408 mAh/g at 0.1 A/g	116 mAh/g (20,000 cycles at 15 A/g)	[111]
		TiN@V_2O_5 core-shell	636 mAh/g at 0.5 mA/cm^2	90.6% retention (3,500 cycles at 8 mA/cm^2)	[113]
Composite construction	combine the advantages and synergistic effects between the different components	V_3O_7/V_2O_5	306 mAh/g at 0.5 A/g	17.4% fading (6,500 at 5 A/g)	[118]
		MnO_2/graphene	301 mAh/g at 0.5 A/g	64.1% retention (300 cycle at 20 mA/cm^2)	[123]
		$V_2O_5{\cdot}nH_2O$-graphene	466 mAh/g at 0.1 A/g	100% retention (5,000 cycle at 10 A/g)	[25]

doi.org/10.1002/elsa.202100090

terms of the modification strategy, structural engineering, capacity, and cyclic stability. It is obvious that the electrochemical performance of the cathode materials can be effectively improved through these different strategies.

5 | CONCLUSION AND OUTLOOK

ZIBs have been attracting ever-increasing attention, due to the low cost, environmental benignity, high safety, and high energy density. Despite substantial progress in recent years, to render ZIBs competitive to LIBs in energy storage, rational design of the cathode materials is of great significance to further improve the ZIB performance. Toward this end, a range of critical roadblocks needs to be tackled, such as dissolution and structural collapse of cathode materials during cycling, generation of by-products, formation of zinc dendrite, corrosion of zinc anode, and hydrogen evolution. In this review, the recent cathode-based strategies are summarized to address the issues of active materials dissolution, degradation of electrochemical performance, and structural collapse during cycling. To further enhance the electrochemical performance of ZIBs, addiitonal research is needed, in particular, in the following key areas.

1. Multi-strategies for cathode material engineering. Current research has mostly focused on a single strategy to improve the performance of the cathode materials, and the enhancement is limited (Table 1). Thus, future research should be conducted whereby multiple strategies are combined to enhance the performance of cathode materials through the realization of synergistic effects. Within this context, facile, cost-effective, and simple fabrication processes are needed to achieve multi-modification of the cathode materials.
2. Reaction kinetics in cathode materials. Since the electrochemical properties of cathode materials are significantly affected by the reaction kinetics, attention should be focused on enhancing the Zn ion transport kinetics in the cathode materials. The ionic diffusion coefficients, pseudocapacitive behaviors, Zn-ion migration paths, and energy barriers should be taken into consideration in the design of cathode materials. For example, the large contribution of pseudocapacitance in cathode materials will lead to a high rate capability and long cycle life, which can be achieved through the construction of nanosized cathode materials with controllable pores and large specific surface area. Moreover, for the cathode materials based on ion (de)intercalation mechanism, the key point to improve the electrochemical performance is to provide sufficient diffusion space and meanwhile maintain a stable structure, which can be realized through pre-intercalation (interlayer modulation), substitution, or defect engineering.[59] The mechanistic insights of the reaction kinetics in cathode materials will be critical for the rational design of high-performance cathode materials of ZIBs. This should be a focus in future research.
3. Properties of cathode/electrolyte interface. As an essential part of ZIBs, the electrolyte is a bridge that effectively connects the cathode and anode materials during the charge/discharge process. Currently, studies have mostly focused on the selection of a specific electrolyte for ZIBs, while the impacts of the cathode/electrolyte interface on the capacity performance as well as the compatibility between the cathode materials and electrolyte have remained largely unexplored. Advanced characterization tools need to be developed and employed to unravel the microstructure and structural evolution of the cathode/electrolyte interface during the charge/discharge process. Furthermore, coating modification on the cathode surface is beneficial to optimizing the cathode/electrolyte interfacial properties.
4. High mass loading of active materials on cathodes. To achieve a high energy density of ZIBs, high mass-loading cathode materials are needed in battery design. However, with an increased loading of the active materials in cathodes, inevitable issues emerge, such as powder aggregation, low usage efficiency of active materials, and cracking and pulverization, which severely deteriorate the electrochemical performance of the cathode materials. Therefore, effective binders are critically needed to homogenize and strongly adhere the powders of active materials, as well as facile methods to coat high massing-loading active materials onto the current collectors.
5. Smart and miniature devices. With the increasing demand for miniature electronics, energy storage devices need to be smarter, smaller, more flexible, and more portable. Thus, extensive efforts should be devoted to the design of cathode materials with high flexibility, high wearability, and lightweight to meet the ever-increasing demand for functional ZIBs. Moreover, free-standing cathode materials without any binder can improve the structural stability and reduce the interface resistance of electrodes, a unique feature for the application in smart ZIB devices.
6. Development of advanced in-situ characterization and simulation methods. In situ characterization methods can clearly probe the dynamic process of Zn ion diffusion into/from cathode materials, and shed light on the energy storage mechanism of ZIBs. Moreover, DFT simulation methods can greatly contribute to a deep understanding of the intrinsic properties of cathode materials as well as the energy storage mechanism, which are

essential for the development of high-performance ZIB systems. Thus, simulation methods, including high-throughput computational simulation, deep learning, and even artificial intelligence, need to be developed for the rational design of high-performance cathodes, exploration of potential cathode candidates for ZIBs, and deep understanding of the energy storage mechanism in ZIBs.

In addition to the cathode materials, the effects of the Zn metal anode, electrolyte, and separator on the performance of ZIBs should also be carefully investigated. In terms of the Zn metal anode, effective strategies are required to hinder the growth of dendrites, alleviate the dissolution, prevent side reactions, and enhance the stability during cycling, so as to achieve high-performance ZIBs. Meanwhile, electrolytes with a wide voltage window, high compatibility with electrode materials, low toxicity, and low cost are also urgently needed. Research along these directions is ongoing, particularly on the feasibility and applicability of ZIBs in high-performance energy storage systems.

ACKNOWLEDGMENTS

P.G.H. acknowledges support from the Beijing Natural Science Foundation (2204086). S.W.C. thanks the National Science Foundation for partial support of the work (CHE-1900235 and CHE-2003685).

REFERENCES

1. L. Lu, X. Han, J. Li, J. Hua, M. Ouyang, *J. Power Sources* **2013**, *226*, 272.
2. P. He, Z. Ding, X. Zhao, J. Liu, S. Yang, P. Gao, L.-Z. Fan, *Inorg. Chem.* **2019**, *58*, 12724.
3. J. Vetter, P. Novák, M. R. Wagner, C. Veit, K.-C. Möller, J. Besenhard, M. Winter, M. Wohlfahrt-Mehrens, C. Vogler, A. Hammouche, *J. Power Sources* **2005**, *147*, 269.
4. K. Liu, Y. Liu, D. Lin, A. Pei, Y. Cui, *Sci. Adv.* **2018**, *4*, eaas9820.
5. T. Jiang, P. He, Y. Liang, L.-Z. Fan, *Chem. Eng. J.* **2021**, 129965.
6. K. Kubota, M. Dahbi, T. Hosaka, S. Kumakura, S. Komaba, *Chem. Rec.* **2018**, *18*, 459.
7. Q. Huang, Y. Feng, S. Xu, L. Xiao, P. He, X. Ji, P. Wang, L. Zhou, W. Wei, *ChemElectroChem* **2020**, *7*, 4383.
8. M. J. Park, H. Yaghoobnejad Asl, A. Manthiram, *ACS Energy Lett*. **2020**, *5*, 2367.
9. C. Xu, B. Li, H. Du, F. Kang, *Angew. Chem.* **2012**, *124*, 957.
10. B. Tang, L. Shan, S. Liang, J. Zhou, *Energy Environ. Sci.* **2019**, *12*, 3288.
11. B. Yong, D. Ma, Y. Wang, H. Mi, C. He, P. Zhang, *Adv. Energy Mater.* **2020**, *10*, 2002354.
12. C. Li, X. Zhang, W. He, G. Xu, R. Sun, *J. Power Sources* **2020**, *449*, 227596.
13. A. Konarov, N. Voronina, J. H. Jo, Z. Bakenov, Y.-K. Sun, S.-T. Myung, *ACS Energy Lett*. **2018**, *3*, 2620.
14. X. Jia, C. Liu, Z. G. Neale, J. Yang, G. Cao, *Chem. Rev.* **2020**, *120*, 7795.
15. N. Zhang, X. Chen, M. Yu, Z. Niu, F. Cheng, J. Chen, *Chem. Soc. Rev.* **2020**, *49*, 4203.
16. D. Chen, M. Lu, D. Cai, H. Yang, W. Han, *J. Energy Chem.* **2021**, *54*, 712
17. X. Zhao, L. Mao, Q. Cheng, F. Liao, G. Yang, X. Lu, L. Chen, *Energy Storage Mater*. **2021**, *38*, 397.
18. Z. Liu, H. Sun, L. Qin, X. Cao, J. Zhou, A. Pan, G. Fang, S. Liang, *ChemNanoMat* **2020**, *6*, 1553.
19. T. Xiong, Y. Zhang, W. S. V. Lee, J. Xue, *Adv. Energy Mater.* **2020**, *10*, 2001769.
20. M. E. Pam, D. Yan, J. Yu, D. Fang, L. Guo, X. L. Li, T. C. Li, X. Lu, L. K. Ang, R. Amal, *Adv.Sci*. **2021**, *8*, 2002722.
21. J. Huang, Z. Wang, M. Hou, X. Dong, Y. Liu, Y. Wang, Y. Xia, *Nat. Commun.* **2018**, *9*, 2906.
22. N. Zhang, F. Cheng, Y. Liu, Q. Zhao, K. Lei, C. Chen, X. Liu, J. Chen, *J. Am. Chem. Soc.* **2016**, *138*, 12894.
23. D. Zhang, J. Cao, X. Zhang, N. Insin, S. Wang, J. Han, Y. Zhao, J. Qin, Y. Huang, *Adv. Funct. Mater.* **2021**, 2009412.
24. H. Wang, S. Zhang, C. Deng, *ACS Appl. Mater. Interfaces* **2019**, *11*, 35796.
25. H. Luo, B. Wang, F. Wu, J. Jian, K. Yang, F. Jin, B. Cong, Y. Ning, Y. Zhou, D. Wang, H. Liu, S. Dou, *Nano Energy* **2021**, *81*, 105601.
26. D. Selvakumaran, A. Pan, S. Liang, G. Cao, *J. Mater. Chem. A* **2019**, *7*, 18209.
27. L. Chen, Q. An, L. Mai, *Adv. Mater. Interfaces* **2019**, *6*, 1900387.
28. B. Liu, Y. Sun, L. Liu, S. Xu, X. Yan, *Adv. Funct. Mater.* **2018**, *28*, 1704973.
29. H. Qin, L. Chen, L. Wang, X. Chen, Z. Yang, *Electrochim. Acta* **2019**, *306*, 307.
30. L. Shan, J. Zhou, W. Zhang, C. Xia, S. Guo, X. Ma, G. Fang, X. Wu, S. Liang, *Energy Technol*. **2019**, *7*, 1900022.
31. P. He, J. Liu, X. Zhao, Z. Ding, P. Gao, L.-Z. Fan, *J. Mater. Chem. A* **2020**, *8*, 10370.
32. F. Liu, Z. Chen, G. Fang, Z. Wang, Y. Cai, B. Tang, J. Zhou, S. Liang, *Nano-Micro Lett.* **2019**, *11*, 25.
33. Q. Zhu, Q. Xiao, B. Zhang, Z. Yan, X. Liu, S. Chen, Z. Ren, Y. Yu, *J. Mater. Chem. A* **2020**, *8*, 10761.
34. K. Hurlbutt, S. Wheeler, I. Capone, M. Pasta, *Joule* **2018**, *2*, 1950.
35. G. Zampardi, F. La Mantia, *Current Opinion in Electrochemistry* **2020**, *21*, 84.
36. Q. Yang, F. Mo, Z. Liu, L. Ma, X. Li, D. Fang, S. Chen, S. Zhang, C. Zhi, *Adv. Mater.* **2019**, *31*, 1901521.
37. G. Kasiri, R. Trócoli, A. B. Hashemi, F. La Mantia, *Electrochim. Acta* **2016**, *222*, 74.
38. Z. Guo, Y. Ma, X. Dong, J. Huang, Y. Wang, Y. Xia, *Angew. Chem. Int. Ed.* **2018**, *57*, 11737.
39. D. Kundu, P. Oberholzer, C. Glaros, A. Bouzid, E. Tervoort, A. Pasquarello, M. Niederberger, *Chem. Mater.* **2018**, *30*, 3874.
40. Q. Zhao, W. Huang, Z. Luo, L. Liu, Y. Lu, Y. Li, L. Li, J. Hu, H. Ma, J. Chen, *Sci. Adv.* **2018**, *4*, eaao1761.
41. H. Liang, Z. Cao, F. Ming, W. Zhang, D. H. Anjum, Y. Cui, L. Cavallo, H. N. Alshareef, *Nano Lett*. **2019**, *19*, 3199.
42. L. Ma, S. Chen, H. Li, Z. Ruan, Z. Tang, Z. Liu, Z. Wang, Y. Huang, Z. Pei, J. A. Zapien, *Energy Environ. Sci.* **2018**, *11*, 2521.
43. X. He, H. Zhang, X. Zhao, P. Zhang, M. Chen, Z. Zheng, Z. Han, T. Zhu, Y. Tong, X. Lu, *Adv. Sci.* **2019**, *6*, 1900151.
44. L. Chen, Z. Yang, H. Qin, X. Zeng, J. Meng, *J. Power Sources* **2019**, *425*, 162.

45. J. Ding, Z. Du, L. Gu, B. Li, L. Wang, S. Wang, Y. Gong, S. Yang, *Adv. Mater.* **2018**, *30*, 1800762.
46. X. Zhang, Y. Tang, P. He, Z. Zhang, T. Chen, *Carbon* **2021**, *172*, 207.
47. M. H. Alfaruqi, V. Mathew, J. Gim, S. Kim, J. Song, J. P. Baboo, S. H. Choi, J. Kim, *Chem. Mater.* **2015**, *27*, 3609.
48. Y. Zhang, F. Wan, S. Huang, S. Wang, Z. Niu, J. Chen, *Nat. Commun.* **2020**, *11*, 2199.
49. Y. Li, Z. Huang, P. K. Kalambate, Y. Zhong, Z. Huang, M. Xie, Y. Shen, Y. Huang, *Nano Energy* **2019**, *60*, 752.
50. W. S. V. Lee, T. Xiong, X. Wang, J. Xue, *Small Methods* **2021**, *5*, 2000815.
51. P. He, M. Yan, G. Zhang, R. Sun, L. Chen, Q. An, L. Mai, *Adv. Energy Mater.* **2017**, *7*, 1601920.
52. G. Li, Z. Yang, Y. Jiang, C. Jin, W. Huang, X. Ding, Y. Huang, *Nano Energy* **2016**, *25*, 211.
53. H. Pan, Y. Shao, P. Yan, Y. Cheng, K. S. Han, Z. Nie, C. Wang, J. Yang, X. Li, P. Bhattacharya, *Nat. Energy* **2016**, *1*, 16039.
54. K. Zhu, T. Wu, S. Sun, W. van den Bergh, M. Stefik, K. Huang, *Energy Storage Mater*. **2020**, *29*, 60.
55. X. Gao, H. Wu, W. Li, Y. Tian, Y. Zhang, H. Wu, L. Yang, G. Zou, H. Hou, X. Ji, *Small* **2020**, *16*, 1905842.
56. W. Sun, F. Wang, S. Hou, C. Yang, X. Fan, Z. Ma, T. Gao, F. Han, R. Hu, M. Zhu, *J. Am. Chem. Soc.* **2017**, *139*, 9775.
57. D. Kundu, B. D. Adams, V. Duffort, S. H. Vajargah, L. F. Nazar, *Nat. Energy* **2016**, *1*, 16132.
58. N. Zhang, Y. Dong, Y. Wang, Y. Wang, J. Li, J. Xu, Y. Liu, L. Jiao, F. Cheng, *ACS Appl. Mater. Interfaces* **2019**, *11*, 32978.
59. Y. Tan, F. An, Y. Liu, S. Li, P. He, N. Zhang, P. Li, X. Qu, *J. Power Sources* **2021**, *492*, 229655.
60. L. E. Blanc, D. Kundu, L. F. Nazar, *Joule* **2020**, *4*, 77.
61. J. Ming, J. Guo, C. Xia, W. Wang, H. N. Alshareef, *Mater. Sci. Engineering: R: Reports* **2019**, *135*, 58.
62. G. Liu, H. Huang, R. Bi, X. Xiao, T. Ma, L. Zhang, *J. Mater. Chem. A* **2019**, *7*, 20806.
63. Q. Chen, J. Jin, Z. Kou, C. Liao, Z. Liu, L. Zhou, J. Wang, L. Mai, *Small* **2020**, *16*, 2000091.
64. J. Zeng, Z. Zhang, X. Guo, G. Li, *J. Mater. Chem. A* **2019**, *7*, 21079.
65. Y. Liu, Z. Pan, D. Tian, T. Hu, H. Jiang, J. Yang, J. Sun, J. Zheng, C. Meng, Y. Zhang, *Chem. Eng. J.* **2020**, *399*, 125842.
66. T. Wei, Q. Li, G. Yang, C. Wang, *Electrochim. Acta* **2018**, *287*, 60.
67. J. Shin, D. S. Choi, H. J. Lee, Y. Jung, J. W. Choi, *Adv. Energy Mater.* **2019**, *9*, 1900083.
68. S. Chen, Y. Zhang, H. Geng, Y. Yang, X. Rui, C. C. Li, *J. Power Sources* **2019**, *441*, 227192.
69. Y. Yang, Y. Tang, S. Liang, Z. Wu, G. Fang, X. Cao, C. Wang, T. Lin, A. Pan, J. Zhou, *Nano Energy* **2019**, *61*, 617.
70. G. Su, S. Chen, H. Dong, Y. Cheng, Q. Liu, H. Wei, E. H. Ang, H. Geng, C. C. Li, *Nanoscale* **2021**, *13*, 2399.
71. P. He, G. Zhang, X. Liao, M. Yan, X. Xu, Q. An, J. Liu, L. Mai, *Adv. Energy Mater.* **2018**, *8*, 1702463.
72. Y. Yang, Y. Tang, G. Fang, L. Shan, J. Guo, W. Zhang, C. Wang, L. Wang, J. Zhou, S. Liang, *Energy Environ. Sci.* **2018**, *11*, 3157.
73. F. Ming, H. Liang, Y. Lei, S. Kandambeth, M. Eddaoudi, H. N. Alshareef, *ACS Energy Lett*. **2018**, *3*, 2602.
74. T. Hu, Z. Feng, Y. Zhang, Y. Liu, J. Sun, J. Zheng, H. Jiang, P. Wang, X. Dong, C. Meng, *Inorg. Chem. Front.* **2021**, *8*, 79.
75. J. Zheng, C. Liu, M. Tian, X. Jia, E. P. Jahrman, G. T. Seidler, S. Zhang, Y. Liu, Y. Zhang, C. Meng, *Nano Energy* **2020**, *70*, 104519.
76. L. Xu, Y. Zhang, J. Zheng, H. Jiang, T. Hu, C. Meng, *Mater. Today Energy* **2020**, *18*, 100509.
77. D. Bin, W. Huo, Y. Yuan, J. Huang, Y. Liu, Y. Zhang, F. Dong, Y. Wang, Y. Xia, *Chem*. **2020**, *6*, 968.
78. S. Liu, H. Zhu, B. Zhang, G. Li, H. Zhu, Y. Ren, H. Geng, Y. Yang, Q. Liu, C. C. Li, *Adv. Mater.* **2020**, *32*, 2001113.
79. S. Chen, K. Li, K. S. Hui, J. Zhang, *Adv. Funct. Mater.* **2020**, *30*, 2003890.
80. M. Wang, J. Zhang, L. Zhang, J. Li, W. Wang, Z. Yang, L. Zhang, Y. Wang, J. Chen, Y. Huang, *ACS Appl. Mater. Interfaces* **2020**, *12*, 31564.
81. V. Verma, S. Kumar, W. Manalastas Jr, J. Zhao, R. Chua, S. Meng, P. Kidkhunthod, M. Srinivasan, *ACS Appl. Energy Mater.* **2019**, *2*, 8667.
82. Y. Du, X. Wang, J. Sun, *Nano Research* **2021**, *14*, 754.
83. M. Li, Z. Li, X. Wang, J. Meng, X. Liu, B.-k. Wu, C. Han, L. Mai, *Energy Environ. Sci.* **2021**, https://doi.org/10.1039/d1ee00030f.
84. M. Yan, P. He, Y. Chen, S. Wang, Q. Wei, K. Zhao, X. Xu, Q. An, Y. Shuang, Y. Shao, *Adv. Mater.* **2018**, *30*, 1703725.
85. J. Lai, H. Zhu, X. Zhu, H. Koritala, Y. Wang, *ACS Appl. Energy Mater* **2019**, *2*, 1988.
86. V. Soundharrajan, B. Sambandam, S. Kim, M. H. Alfaruqi, D. Y. Putro, J. Jo, S. Kim, V. Mathew, Y.-K. Sun, J. Kim, *Nano Lett*. **2018**, *18*, 2402.
87. Q. Li, T. Wei, K. Ma, G. Yang, C. Wang, *ACS Appl. Mater. Interfaces* **2019**, *11*, 20888.
88. P. He, Y. Quan, X. Xu, M. Yan, W. Yang, Q. An, L. He, L. Mai, *Small* **2017**, *13*, 1702551.
89. N. Zhang, Y. Dong, M. Jia, X. Bian, Y. Wang, M. Qiu, J. Xu, Y. Liu, L. Jiao, F. Cheng, *ACS Energy Lett*. **2018**, *3*, 1366.
90. Y. Tao, Z. Li, L. Tang, X. Pu, T. Cao, D. Cheng, Q. Xu, H. Liu, Y. Wang, Y. Xia, *Electrochim. Acta* **2020**, *331*, 135296.
91. J. Zhou, A. Dong, L. Du, C. Yang, L. Ye, X. Wang, L. Zhao, Q. Jiang, *Chem. Eng. J.* **2020**, 127770.
92. J. H. Jo, Y.-K. Sun, S.-T. Myung, *J. Mater. Chem. A* **2017**, *5*, 8367.
93. B. Lan, Z. Peng, L. Chen, C. Tang, S. Dong, C. Chen, M. Zhou, C. Chen, Q. An, P. Luo, *J. Alloys Compd.* **2019**, *787*, 9.
94. Y. Zhang, S. Deng, M. Luo, G. Pan, Y. Zeng, X. Lu, C. Ai, Q. Liu, Q. Xiong, X. Wang, *Small* **2019**, *15*, 1905452.
95. D. Wang, S. Wang, Z. Lu, *Int. J. Energy Res.* **2021**, *45*, 2498.
96. L. Chen, Z. Yang, F. Cui, J. Meng, Y. Jiang, J. Long, X. Zeng, *Mater. Chem. Front.* **2020**, *4*, 213.
97. Y. Fu, Q. Wei, G. Zhang, X. Wang, J. Zhang, Y. Hu, D. Wang, L. Zuin, T. Zhou, Y. Wu, S. Sun, *Adv. Energy Mater.* **2018**, *8*, 1801445.
98. X. Wang, L. Ye, Y. Zou, L. Zhao, Q. Jiang, *Mater. Today Energy* **2021**, *19*, 100593.
99. T. Xiong, Z. G. Yu, H. Wu, Y. Du, Q. Xie, J. Chen, Y. W. Zhang, S. J. Pennycook, W. S. V. Lee, J. Xue, *Adv. Energy Mater.* **2019**, *9*, 1803815.
100. Y. Zhang, L. Tao, C. Xie, D. Wang, Y. Zou, R. Chen, Y. Wang, C. Jia, S. Wang, *Adv. Mater.* **2020**, *32*, 1905923.
101. Y. Zhang, S. Deng, M. Luo, G. Pan, Y. Zeng, X. Lu, C. Ai, Q. Liu, Q. Xiong, X. Wang, X. Xia, J. Tu, *Small* **2019**, *15*, 1905452.
102. M. Liao, J. Wang, L. Ye, H. Sun, Y. Wen, C. Wang, X. Sun, B. Wang, H. Peng, *Angew. Chem.* **2020**, *132*, 2293.
103. Z. Li, Y. Ren, L. Mo, C. Liu, K. Hsu, Y. Ding, X. Zhang, X. Li, L. Hu, D. Ji, G. Cao, *ACS Nano* **2020**, *14*, 5581.

104. C. Zhu, G. Fang, S. Liang, Z. Chen, Z. Wang, J. Ma, H. Wang, B. Tang, X. Zheng, J. Zhou, *Energy Storage Mater*. **2020**, *24*, 394.
105. P. He, S. Chen, *ChemElectroChem* **2021**, *8*, 783.
106. H. T. Tan, X. Rui, W. Sun, Q. Yan, T. M. Lim, *Nanoscale* **2015**, *7*, 14595.
107. F. Liu, Z. Chen, G. Fang, Z. Wang, Y. Cai, B. Tang, J. Zhou, S. Liang, *Nano-Micro Lett.* **2019**, *11*, 25.
108. D. Xu, H. Wang, F. Li, Z. Guan, R. Wang, B. He, Y. Gong, X. Hu, *Adv. Mater. Interfaces* **2019**, *6*, 1801506.
109. J. Kim, S. H. Lee, C. Park, H.-S. Kim, J.-H. Park, K. Y. Chung, H. Ahn(**2021**). *Adv. Funct. Mater.*, *31*, 2100005.
110. T. Wei, Y. Liu, G. Yang, C. Wang, *Energy Storage Mater*. **2020**, *30*, 130.
111. L. Chen, Z. Yang, Y. Huang, *Nanoscale* **2019**, *11*, 13032.
112. L. Wang, K.-W. Huang, J. Chen, J. Zheng, *Sci. Adv.* **2019**, *5*, eaax4279.
113. Q. Li, Q. Zhang, C. Liu, Z. Zhou, C. Li, B. He, P. Man, X. Wang, Y. Yao, *J. Mater. Chem. A* **2019**, *7*, 12997.
114. B. Wu, W. Luo, M. Li, L. Zeng, L. Mai, *Nano Research* **2021**, . https://doi.org/10.1007/s12274-021-3392-1.
115. X. Dai, F. Wan, L. Zhang, H. Cao, Z. Niu, *Energy Storage Mater.* **2019**, *17*, 143.
116. Q. Zhang, Y. Wang, B. Zhang, K. Zhao, P. He, B. Huang, *Carbon* **2018**, *127*, 449.
117. S. Islam, M. H. Alfaruqi, J. Song, S. Kim, D. T. Pham, J. Jo, S. Kim, V. Mathew, J. P. Baboo, Z. Xiu, J. Kim, *J. Energy Chem.* **2017**, *26*, 815.
118. H. Chen, L. Chen, J. Meng, Z. Yang, J. Wu, Y. Rong, L. Deng, Y. Shi, *J. Power Sources* **2020**, *474*, 228569.
119. M. Qin, W. Liu, L. Shan, G. Fang, X. Cao, S. Liang, J. Zhou, *J. Electroanal. Chem.* **2019**, *847*, 113246.
120. G. Xiong, P. He, Z. Lyu, T. Chen, B. Huang, L. Chen, T. S. Fisher, *Nat. Commun.* **2018**, *9*, 790.
121. N. Palaniyandy, M. A. Kebede, K. Raju, K. I. Ozoemena, L. le Roux, M. K. Mathe, R. Jayaprakasam, *Mater. Chem. Phys.* **2019**, *230*, 258.
122. Z. Pan, J. Yang, J. Yang, Q. Zhang, H. Zhang, X. Li, Z. Kou, Y. Zhang, H. Chen, C. Yan, J. Wang, *ACS Nano* **2020**, *14*, 842.
123. C. Wang, Y. Zeng, X. Xiao, S. Wu, G. Zhong, K. Xu, Z. Wei, W. Su, X. Lu, *J. Energy Chem.* **2020**, *43*, 182.
124. S. Islam, M. H. Alfaruqi, J. Song, S. Kim, D. T. Pham, J. Jo, S. Kim, V. Mathew, J. P. Baboo, Z. Xiu, *J. Energy Chem.* **2017**, *26*, 815.
125. F. Xing, X. Shen, Y. Chen, X. Liu, T. Chen, Q. Xu, *Dalton Trans.* **2021**, *50*, 5795.

AUTHOR BIOGRAPHIES

Pingge He received her B.S. and Ph.D. degrees in materials science and engineering from Central South University (China) in 2012 and 2017, respectively. During her Ph.D. study, she visited the Birck Nanotechnology Center of Purdue University from 2014 to 2017. After that, she was appointed as an associate professor at the University of Science and Technology Beijing (China) in 2018. Currently, she is doing her postdoctoral research in Prof. Shaowei Chen's group at the University of California-Santa Cruz, which is focused on carbon nanostructures and applications in electrochemical energy storage and electrocatalysis.

Shaowei Chen received his B.S. degree in chemistry from the University of Science and Technology of China in 1991, and M.S. and Ph.D. degrees from Cornell University in 1993 and 1996, respectively. Following a postdoctoral appointment at the University of North Carolina – Chapel Hill, he started his independent career in Southern Illinois University in 1998. He moved to the University of California – Santa Cruz in 2004 and is currently a professor of chemistry and the Faculty Director of the UCSC COSMOS program. His research is primarily focused on the electron-transfer chemistry of functional nanomaterials, and applications in electrocatalysis and antimicrobials.

How to cite this article: He P, Chen S. Cathode strategies to improve the performance of zinc-ion batteries. *Electrochem Sci Adv.* **2022**, *2,* e2100090. https://doi.org/10.1002/elsa.202100090